Supplementary Material for

Copper(II) Activation of Nitrite: Nitrosation of Nucleophiles and Generation of NO by Thiols

Subrata Kundu,* William Y. Kim, Jeffery A. Bertke, and Timothy H. Warren*
Department of Chemistry, Georgetown University, Box 571227, Washington, D. C. 20057-1227, United States
*Corresponding author emails: skundu.chem@gmail.com, thw@georgetown.edu

Table of Contents **S1**

1. General Instrumentation and Physical Methods **S2**
2. Materials **S3**
3. Synthesis and Characterization of $[Cl_2NN_{F6}]Cu(\kappa^2\text{-}O_2N)$ (**2**) and $[Cl_2NN_{F6}]Cu(\kappa^2\text{-}O_2N)\bullet THF$ (**2a**) **S4**
4. Reaction of $[Cl_2NN_{F6}]Cu(\kappa^2\text{-}O_2N)\bullet THF$ (**2a**) with two equiv. 4-*tert*-butylbenzylthiol (^{t}BuBnSH) **S6**
5. Reaction of $[Cl_2NN_{F6}]Cu(\kappa^2\text{-}O_2N)\bullet THF$ (**2a**) with two equiv. 1-adamantylthiol (AdSH) **S9**
6. Quantitative NO Trapping by $(TPP)Co^{II}$ Complex **S11**
7. Qualitative NO Trapping by $(dtc)_2Fe^{II}$ Complex **S13**
8. Reaction of $[Cl_2NN_{F6}]Cu(\kappa^2\text{-}O_2N)\bullet THF$ (**2a**) with one equiv. 4-*tert*-butylbenzylthiol (^{t}BuBnSH) **S15**
9. Reaction of $[Cl_2NN_{F6}]Cu(\kappa^2\text{-}O_2N)\bullet THF$ (**2a**) with one equiv. 1-adamantylthiol (AdSH) **S17**
10. Reaction of $[Cl_2NN_{F6}]Cu(\kappa^2\text{-}O_2N)\bullet THF$ (**2a**) with one equiv. trityl thiol (Ph_3CSH) **S18**
11. Reaction of $[Cl_2NN_{F6}]Cu(\kappa^2\text{-}O_2N)\bullet THF$ (**2a**) with *tert*-butanol **S19**
12. Reaction of $[Cl_2NN_{F6}]Cu(\kappa^2\text{-}O_2N)\bullet THF$ (**2a**) with diphenylamine **S21**
13. Reaction of $\{[Cl_2NN_{F6}]Cu\}_2(\mu\text{-}OH)_2$ (**4**) with one equiv. trityl thiol (Ph_3CSH) **S23**
14. Synthesis and Characterization of $[Cl_2NN_{F6}]Cu\text{-}O^tBu$ (**6**) **S24**
15. Reaction of $[Cl_2NN_{F6}]Cu\text{-}O^tBu$ (**6**) with one equiv. thiol (Ph_3CSH) **S26**
16. Reaction of $[Cl_2NN_{F6}]Cu\text{-}SCPh_3$ (**5**) with one equiv. 1-adamantylnitrosothiol (AdSNO) **S27**
17. X-Band EPR spectra of $[Cl_2NN_{F6}]Cu(\kappa^2\text{-}O_2N)\bullet THF$ (**2a**), $[Cl_2NN_{F6}]Cu\text{-}O^tBu$ (**6**), $[Cl_2NN_{F6}]Cu\text{-}SCPh_3$ (**5**) **S28**
18. Crystallographic details and additional structures **S32**
19. References **S40**

1. General Instrumentation and Physical Methods.

The preparation and handling of air-sensitive chemicals were performed under dry nitrogen atmosphere by utilizing MBraun glove-boxes and/or standard Schlenk techniques. ^{1}H, ^{13}C, and ^{19}F NMR spectra were recorded on a Varian 400 MHz spectrometer at room temperature unless otherwise noted. ^{13}C NMR spectra were recorded at 100 MHz. The chemical shift (δ) values are expressed in ppm relative to tetramethylsilane, whereas the residual ^{1}H, ^{13}C signals of the deuterated solvent served as an internal standard. ^{19}F NMR spectra were recorded at 376.0 MHz using an internal reference of $C_6H_5CF_3$ (δ = -63.72 ppm). ^{15}N NMR spectra were recorded at 41.0 MHz and referenced to external standard $Na^{15}NO_2$ in D_2O (609.5 ppm *vs*. liquid NH_3). Elemental analyses were performed on a Perkin-Elmer PE2400 micro-analyzer at Georgetown University. UV-vis spectra were recorded either on a Cary 50 dual beam or Agilent 8454 Diode Array spectrometer equipped with stirrer and Unisoku USP-203 cryostats for variable temperature (-105 °C to 90 °C) experiments. The molar extinction coefficients of different isolated complexes were determined from the Beer's law plot (absorbance *vs* concentration) with at least four different concentrations. IR spectra (with spectral resolution of 2 cm^{-1}) were collected on a Varian 3100 FT-IR spectrometer by using KBr pellet method. The intensities of the vibrational bands are abbreviated as follows: s = strong, m = medium, w = weak, br = broad. Cyclic voltammetry measurements were done at room temperature under dry nitrogen atmosphere of a glove-box using BASi Epsilon Electrochemistry setup with three electrodes (Working electrode: glassy carbon, Auxiliary electrode: platinum wire, Pseudo-reference electrode: silver wire). Details for EPR spectra and X-ray crystallography appear in Sections 17 and 18, respectively.

2. Materials.

All chemicals were purchased from standard vendors (e.g. Sigma-Aldrich, Acros Organics, Strem Chemicals, TCI) and used without further purification unless otherwise mentioned. Molecular sieves (4A, 4-8 mesh beads) were obtained from Fisher Scientific and activated in *vacuo* at 180 °C for 24 h. Extra dry solvents (≥99.5%) with Acroseal® and deuterated solvents were purchased from Acros Organics and Cambridge Isotope Laboratories, respectively. Both anhydrous and deuterated solvents were sparged with nitrogen and stored over activated molecular sieves under nitrogen atmosphere.

$H[Cl_2NN_{F6}]$[1] and $\{[Cl_2NN_{F6}]Cu\}_2(\mu$-toluene)[2] were synthesized according to literature procedures. $Ag^{15}NO_2$ was prepared using commercially available $Na^{15}NO_2$ (98+ atom% ^{15}N from Cambridge Isotope Laboratories) and by following previously published procedures.[3] A solution of $AgNO_3$ (2.19 g, 12.9 mmol) in deionized water (*ca.* 10.0 mL) was added in portions to a vigorously stirring aqueous solution of $Na^{15}NO_2$ (0.902 g, 12.9 mmol) in deionized water (*ca.* 5.0 mL). A faint yellow precipitate of $Ag^{15}NO_2$ started to separate out of the solution immediately. The resultant reaction mixture was kept in the dark for 1 hour. Then the yellow precipitate was collected by suction filtration and washed thoroughly with deionized water (*ca.* 100 mL) and methanol (*ca.* 50 mL). The product was dried under high vacuum to afford $Ag^{15}NO_2$ as a pale yellow powder (1.56 g, 10.1 mmol) in 78% yield. The ^{15}N isotope enrichment in the product was confirmed by comparing the FT-IR spectrum of $Ag^{15}NO_2$ to that of the commercially available $AgNO_2$ (from Strem Chemicals). FT-IR (KBr pellet, cm^{-1}): 848m (^{14}N), 840m (^{15}N).[3]

3. Synthesis and Characterization of $[Cl_2NN_{F6}]Cu(\kappa^2\text{-}O_2N)$ (2) and $[Cl_2NN_{F6}]Cu(\kappa^2\text{-}O_2N)\bullet THF$ (2a).

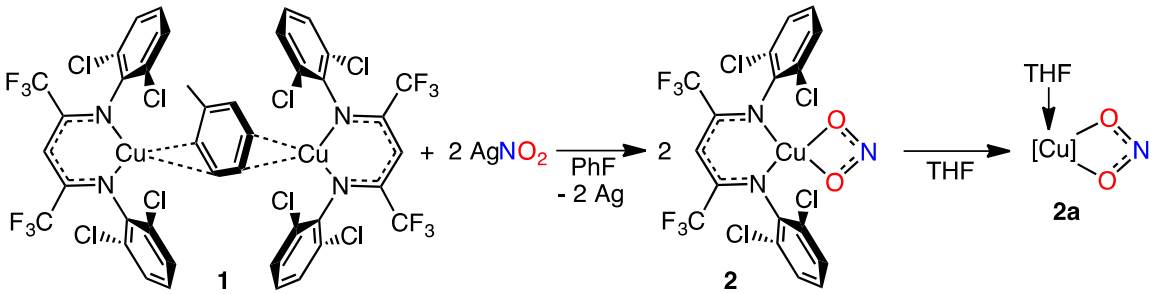

Synthesis of $[Cl_2NN_{F6}]Cu(\kappa^2\text{-}O_2N)$ (2). A suspension of **1** (0.328 g, 0.271 mmol) and 2.2 equiv. $AgNO_2$ (0.092 g, 0.596 mmol) in anhydrous fluorobenzene (5 mL) was stirred at room temperature for 2 h. The resultant dark green reaction mixture was filtered through Celite to remove the insoluble residue. The dark green filtrate thus obtained was evaporated under reduced pressure to afford a green powder **2** (0.247 g, 0.409 mmol) in 75% yield. X-ray quality crystals were grown from a concentrated pentane solution of **2** at -40 °C. Anal. Calcd for $C_{17}H_7F_6N_3O_2Cl_4Cu$ (**2**): C, 33.77; H, 1.17; N, 6.95. Found: C, 34.01; H, 1.31; N, 6.63.

Synthesis and Characterization of $[Cl_2NN_{F6}]Cu(\kappa^2\text{-}O_2N)\bullet THF$ (2a). A tetrahydrofuran bound adduct **2a** can be isolated upon recrystallization of **2** from a concentrated pentane/tetrahydrofuran (10:1) solution (See Figure S26 for X-ray structure). Anal. Calcd for $C_{21}H_{15}F_6N_3O_3Cl_4Cu$ (**2a**): C, 37.27; H, 2.23; N, 6.21. Found: C, 37.02; H, 2.07; N, 6.39. UV-Vis (THF, 25 °C): λ_{max} = 720 nm (ε = 120 $M^{-1}cm^{-1}$) (Figure S1). X-band EPR (pentane, 293 K): g_{iso} = 2.106, A_{iso}(Cu) = 189.0 MHz, A_{iso}(2N) = 29.0 MHz (Figure S20). X-band EPR (pentane, 80 K): g_1 = 2.244, g_2 = 2.036, g_3 = 2.036, A_1(Cu) = 440 MHz, A_2(Cu) = 70 MHz, A_3(Cu) = 20 MHz, A_1(2N) = A_2(2N) = A_3(2N) = 29 MHz (Figure S21).

Crystals of **2a** were used for further reactivity studies due to the presence of one equiv. coordinated tetrahydrofuran which serves as a convenient internal standard for NMR spectroscopic studies.

The synthesis of $[Cl_2NN_{F6}]Cu(\kappa^2\text{-}O_2{}^{15}N)\bullet THF$ (**2a**-^{15}N) employed $Ag^{15}NO_2$ instead of $AgNO_2$.

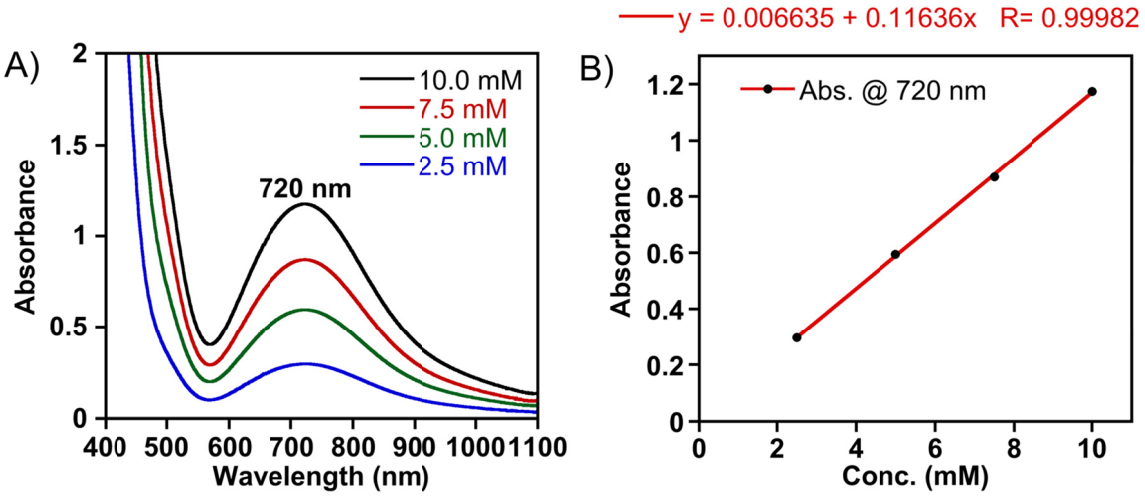

Figure S1. (A) UV-Vis spectra of $[Cl_2NN_{F6}]Cu(\kappa^2\text{-}O_2N)$•THF (**2a**) in tetrahydrofuran at 25 °C at different concentrations. (B) Beer's law plot for **2a** depicts λ_{max}/nm (ε/$M^{-1}cm^{-1}$) = 720 (120).

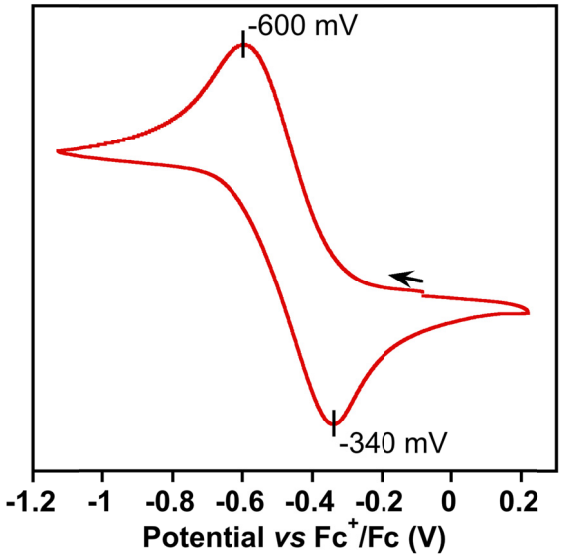

Figure S2. Cyclic voltammogram of $[Cl_2NN_{F6}]Cu(\kappa^2\text{-}O_2N)$•THF (**2a**) (4.0 mM) in tetrahydrofuran at 25 °C in presence of *n*-tetrabutylammonium hexafluorophosphate (2.0 M). Scan proceeds in the indicated direction with scan rate of 25 mV/s.

4. Reaction of $[Cl_2NN_{F6}]Cu(\kappa^2\text{-}O_2N)$•THF (2a) with two equiv. 4-*tert*-butylbenzylthiol (^{t}BuBnSH).

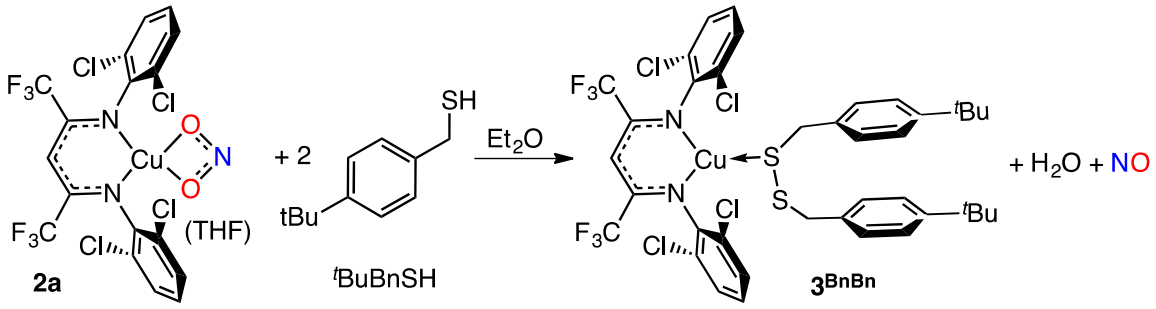

Preparative Scale Reaction.

To a solution of $[Cl_2NN_{F6}]Cu(\kappa^2\text{-}O_2N)$•THF (**2a**) (0.514 g, 0.759 mmol) in Et_2O (5 mL), 4-*tert*-butylbenzylthiol (^{t}BuBnSH) (0.274 g, 1.519 mmol) was added. The color of the solution immediately changed from dark green to orange with concomitant gas evolution (for gas trapping experiments see Sections 6 and 7). After 15 min stirring, the resultant solution was evaporated to afford an orange powder $\mathbf{3^{BnBn}}$ (0.569 g, 0.620 mmol, 82% yield). X-ray quality crystals of $\mathbf{3^{BnBn}}$ (Figure S27) were grown by slow evaporation of a concentrated pentane solution of $\mathbf{3^{BnBn}}$. Anal. calcd. for $C_{39}H_{37}F_6N_2S_2Cl_4Cu$: C, 51.07; H, 4.07; N, 3.05. Found: C, 51.36; H, 4.30; N, 3.19. ^{1}H NMR (400 MHz, 298 K, C_6D_6): δ 7.22 (d, 4H, *m*-Ar-*H*), 7.05 (d, 4H, *o*-Ar-*H*), 6.98 (d, 4H, *m*-Ar-*H*), 6.38 (t, 2H, *p*-Ar-*H*), 6.17 (s, 1H, backbone-C*H*), 3.30 (s, 4H, *CH2*-Ar), 1.18 (s, 18H, ^{t}*Bu*-Ar). ^{19}F NMR (376 MHz, C_6D_6): δ -66.54 (s, -C*F*$_3$). ^{13}C{^{1}H} NMR (100 MHz, C_6D_6): δ 153.69 (q, $^2J_{CF}$ = 27.8 Hz), 150.82, 144.88, 134.11, 129.90, 129.64, 125.73, 125.20, 120.75 (q, $^1J_{CF}$ = 285.9 Hz), 85.39 (m, $^3J_{CF}$ = 4.7 Hz), 43.80, 34.57, 31.43.

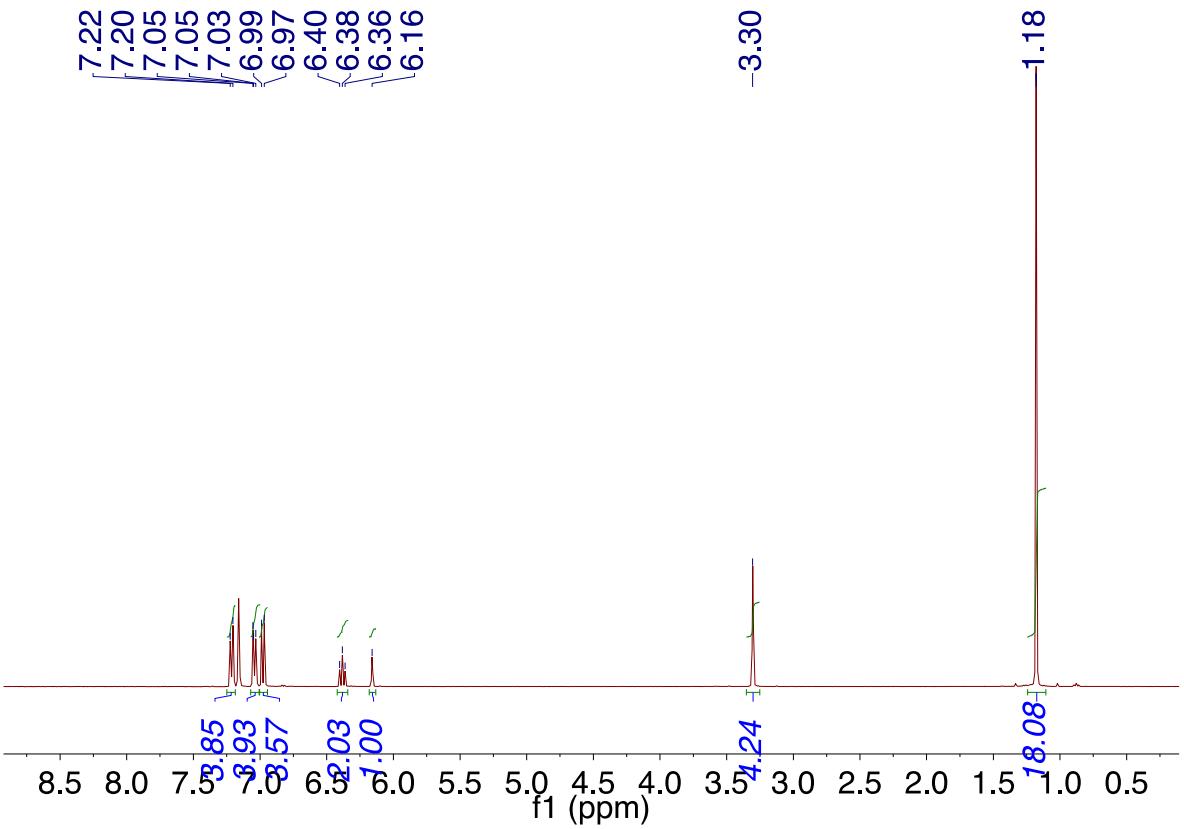

Figure S3. ^{1}H NMR spectrum (400 MHz, 298 K, C_6D_6) of **3**$^{\mathbf{BnBn}}$.

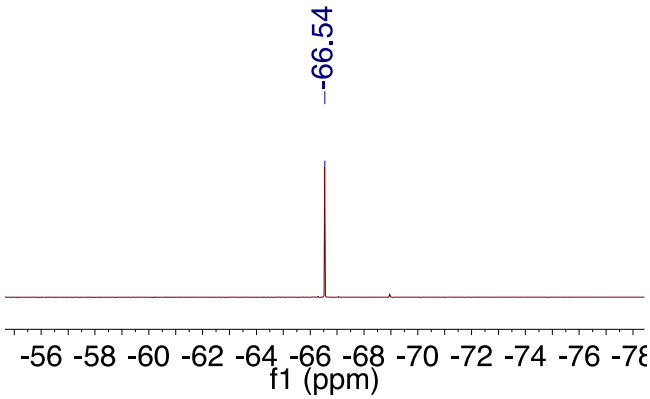

Figure S4. ^{19}F NMR spectrum (376 MHz, 298 K, C_6D_6) of **3**$^{\mathbf{BnBn}}$.

Monitoring the Experiment by NMR.

To a solution of $[Cl_2NN_{F6}]Cu(\kappa^2\text{-}O_2N)\bullet THF$ (**2a**) (48.4 mg, 0.071 mmol) in C_6D_6 (0.5 mL), a solution of 4-*tert*-butylbenzylthiol (^{t}BuBnSH) (25.7 mg, 0.143 mmol, 26.7 µL) in C_6D_6 (0.5 mL) was added. The color of the solution immediately changed from dark green to orange. After 5 min stirring, the resultant solution was analyzed by NMR spectroscopy, which exhibits the formation of $\mathbf{3}^{\mathbf{BnBn}}$ in 80% yield. ^{1}H NMR (400 MHz, 298 K, C_6D_6): 7.22 (d, 4H, *m*-Ar-*H*), 7.05 (d, 4H, *o*-Ar-*H*), 6.98 (d, 4H, *m*-Ar-*H*), 6.38 (t, 2H, *p*-Ar-*H*), 6.17 (s, 1H, backbone-C*H*), 3.32 (s, 4H, *CH2*-Ar), 1.18 (s, 18H, ^{t}*Bu*-Ar).

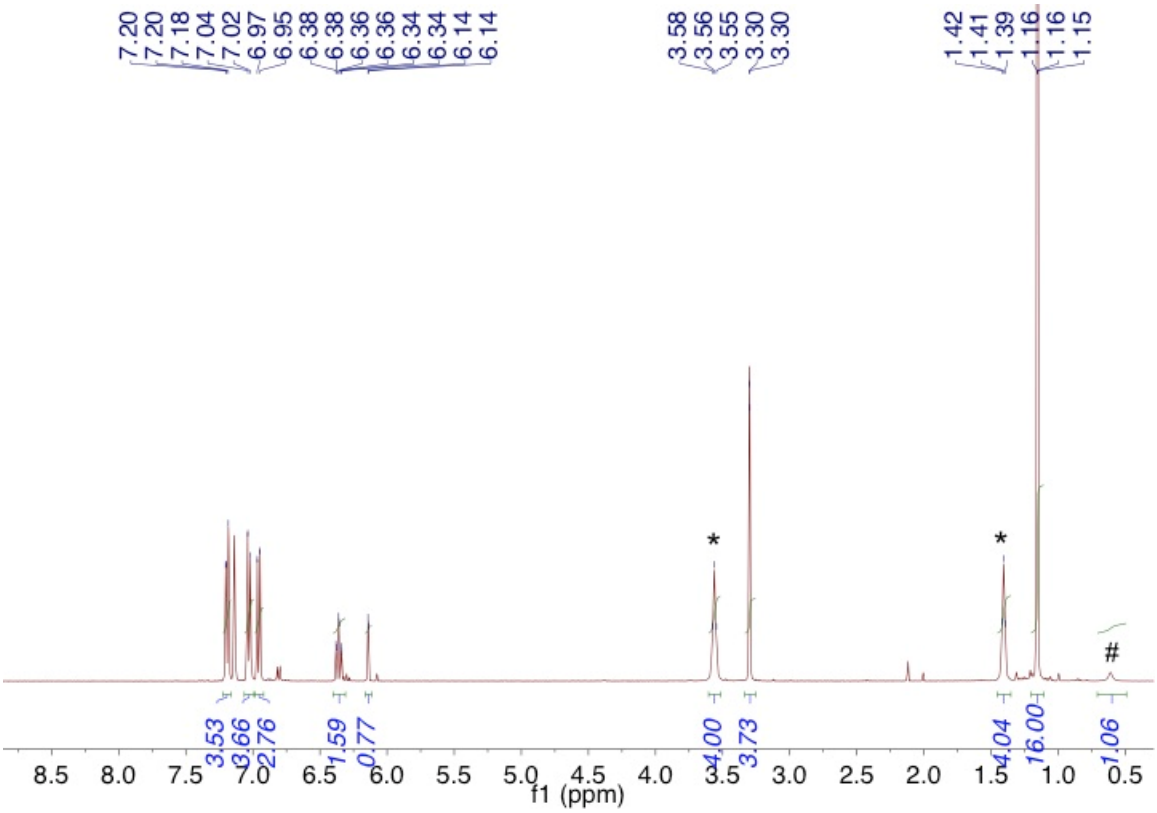

Figure S5. ^{1}H NMR spectrum (400 MHz, 298 K, C_6D_6) of the crude mixture obtained from the reaction of **2a** and ^{t}BuBnSH (2 equiv). One equivalent of tetrahydrofuran originating from **2a** serves as internal standard and peaks are integrated with respect to the four -CH_2O- type protons (from THF) at δ = 3.56 ppm. The resonances marked with * are originating from tetrahydrofuran. The integration of the resonance marked with # provides an NMR yield of 53% for water.

5. Reaction of $[Cl_2NN_{F6}]Cu(\kappa^2\text{-}O_2N)$•THF (2a) with two equiv. 1-adamantylthiol (AdSH).

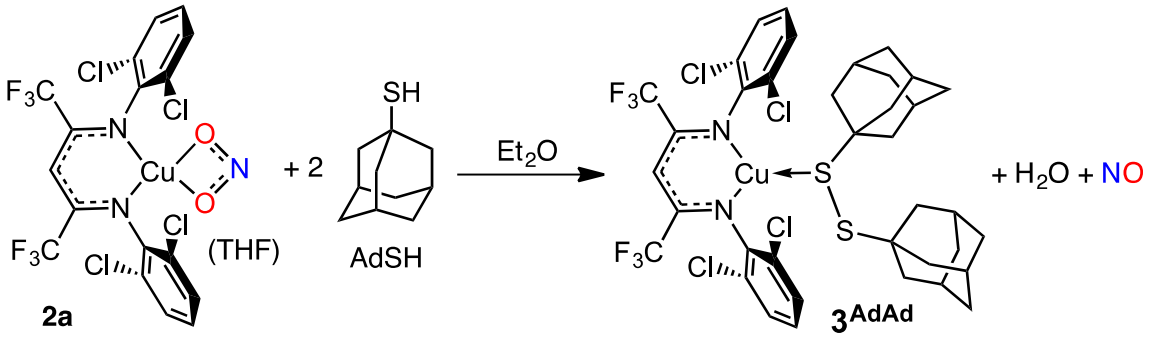

A solution of 1-adamantylthiol (AdSH) (0.327 g, 1.942 mmol) in Et_2O (2 mL) was added to a solution of $[Cl_2NN_{F6}]Cu(\kappa^2\text{-}O_2N)$•THF (**2a**) (0.658 g, 0.972 mmol) in Et_2O (3.0 mL). The color of the solution immediately changed from dark green to orange with simultaneous formation of an orange precipitate and evolution of NO gas (for gas-trapping experiments see Sections 6 and 7). After 15 min stirring, the resultant solution was evaporated to afford an orange powder (0.792 g, 0.886 mmol, 95% yield). X-ray quality crystals of $\mathbf{3}^{\mathbf{AdAd}}$ (Figure S28) were grown by slow evaporation of a saturated Et_2O solution. Anal. calcd. for $C_{37}H_{37}F_6N_2S_2Cl_4Cu$: C, 49.76; H, 4.18; N, 3.14. Found: C, 49.54; H, 4.16; N, 3.51. ^{1}H NMR (400 MHz, 298 K, CD_3CN): δ 7.39 (d, 4H, *m*-Ar-*H*), 7.05 (t, 2H, *p*-Ar-*H*), 5.54 (s, 1H, backbone-C*H*), 2.04 (br, 6H, *CH*-Ad), 1.81 (d, 12H, *CH*$_2$-Ad), 1.68 (m, 12H, *CH*$_2$-Ad). ^{19}F NMR (376 MHz, CD_3CN): δ -66.18 (s, -C*F*$_3$). ^{13}C{^{1}H} NMR (100 MHz, CD_3CN): δ 152.45 (q, $^2J_{CF}$ = 26.6 Hz), 145.23, 129.26, 128.98, 125.78, 121.16 (q, $^1J_{CF}$ = 286.9 Hz), 84.15 (m, $^3J_{CF}$ = 4.8 Hz), 48.10, 43.92, 36.72, 31.04.

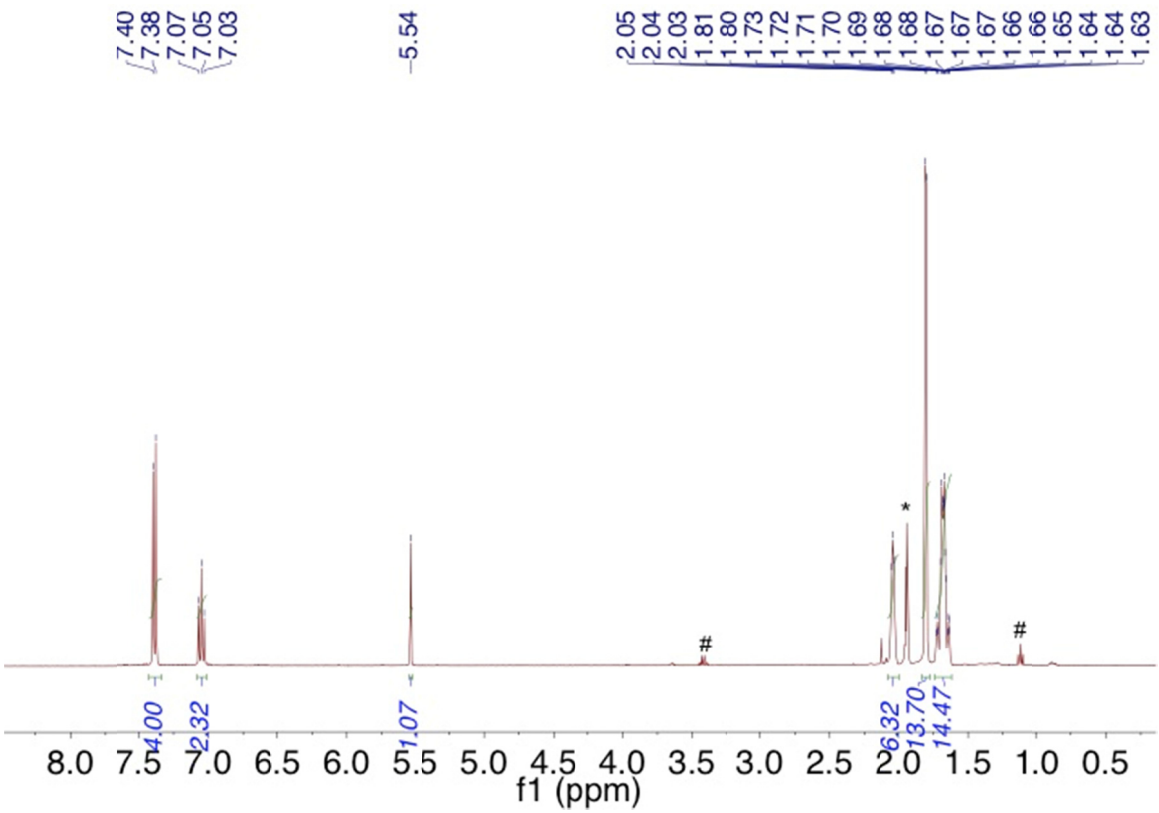

Figure S6. ^{1}H NMR spectrum (400 MHz, 298 K, CD_3CN) of $\mathbf{3}^{\mathbf{AdAd}}$. The resonances marked with * and # are from acetonitrile and trace amount of diethyl ether, respectively.

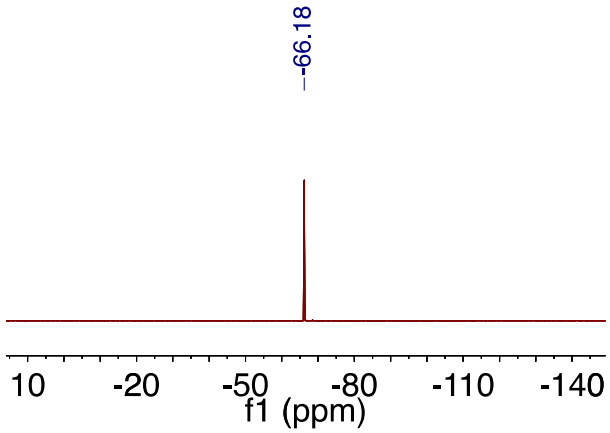

Figure S7. ^{19}F NMR spectrum (376 MHz, 298 K, C_6D_6) of isolated $\mathbf{3}^{\mathbf{AdAd}}$.

6. Quantitative NO Trapping by (TPP)Co^{II} Complex.

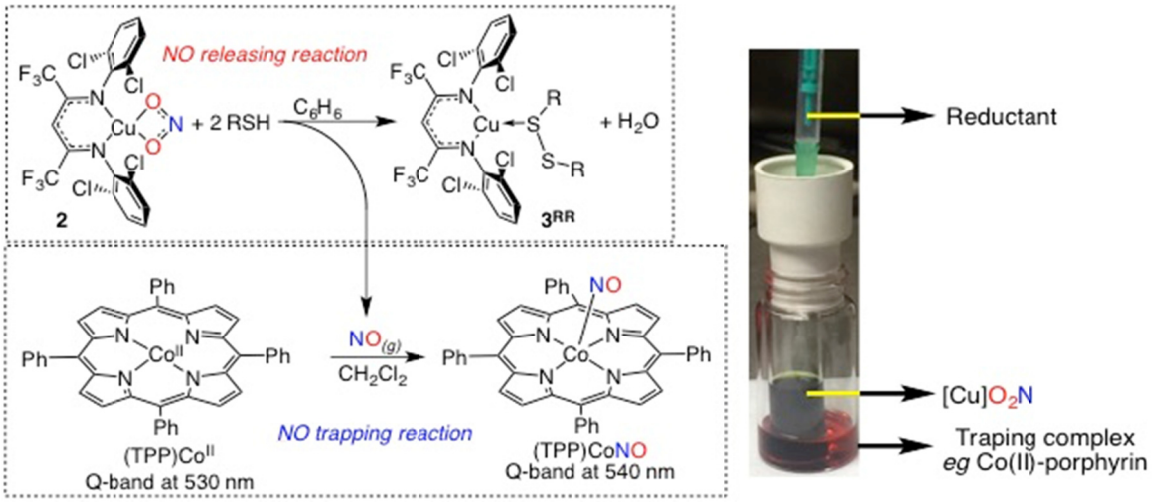

Figure S8. Stoichiometric conversion of (TPP)Co^{II} to (TPP)CoNO utilized for NO quantification.

Cobalt(II) meso-tetraphenylporphine [(TPP)Co^{II}] was purchased from Strem Chemicals and used for quantitative trapping of nitric oxide using a similar experimental set up as previously[4] demonstrated. A smaller vial charged with a solution of **2a** (1.0 mL 10.0 mM) in C_6H_6 was carefully placed in a larger vial containing a solution of (TPP)Co^{II} complex (10.0 mL, 1.0 mM) in CH_2Cl_2 and the bigger vial was sealed with a septum. A solution of 4-*tert*-butylbenzylthiol (^{t}BuBnSH) (1.0 mL 20.0 mM) in C_6H_6 was injected to the inner vial and the vials were gently shaken occasionally for 30 min. Then an aliquot (100 μL) of the resultant (TPP)Co solution from outer vial was diluted to 2.0 mL using CH_2Cl_2 and analyzed by UV-Vis spectroscopy. The Q-band absorption features in the UV-Vis spectra of authentic (TPP)Co^{II} (530 nm) and (TPP)Co(NO) (540 nm) samples were used to compare and quantify the yield of cobalt-nitrosyl species.

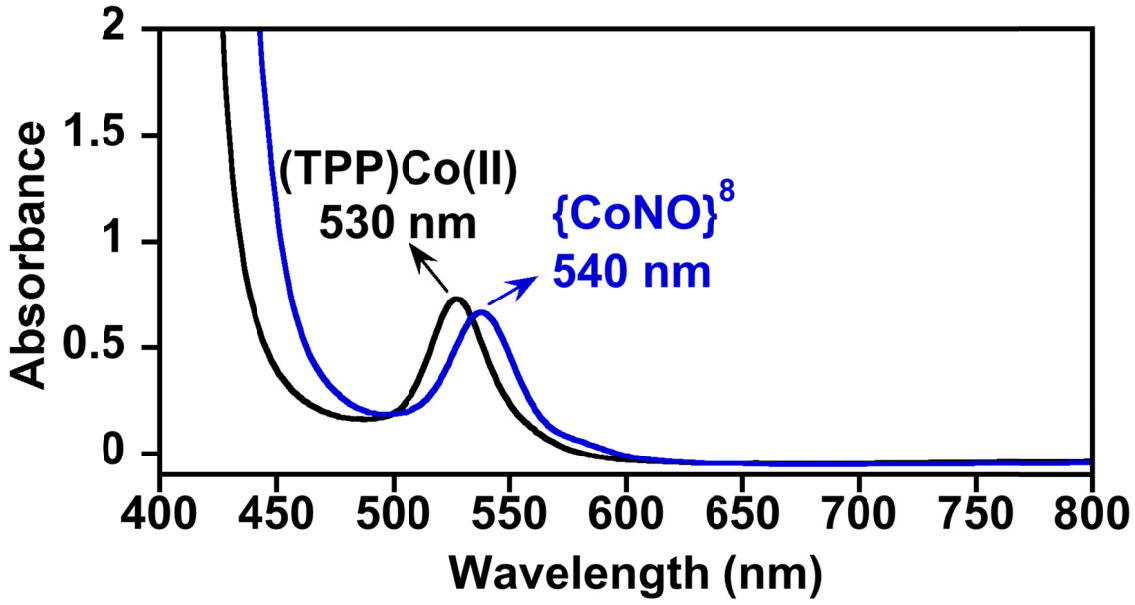

Figure S9. UV-Vis spectra (in CH_2Cl_2 at 25 °C) of [(TPP)Co] (black trace) and [(TPP)Co(NO)] species (blue trace) generated upon reacting [(TPP)Co] with NO released from the mixture of **2a** and (^{t}BuBnSH).

7. Qualitative NO Trapping by $(dtc)_2Fe^{II}$ Complex.

Bis(N,N-diethyldithiocarbamato)iron(II) [$(dtc)_2Fe^{II}$] complex has been used in the literature[5] for trapping nitric oxide. $(dtc)_2Fe^{II}$ was synthesized through a slight modification of a previously[6] reported procedure. An overnight reaction of $FeSO_4 \bullet 7H_2O$ (216.9 mg, 0.78 mmol) and diethylammonium diethyldithiocarbamate (347.1 mg, 1.56 mmol) in dichloromethane (10 mL) resulted in a dark brown solution. The resultant reaction mixture was filtered to remove any insoluble byproduct and the brown filtrate thus obtained was evaporated to dryness under reduced pressure to afford a brown solid. The desired complex [$(dtc)_2Fe^{II}$] was recrystallized from diethyl ether to obtain a brown microcrystalline powder in 71% yield.

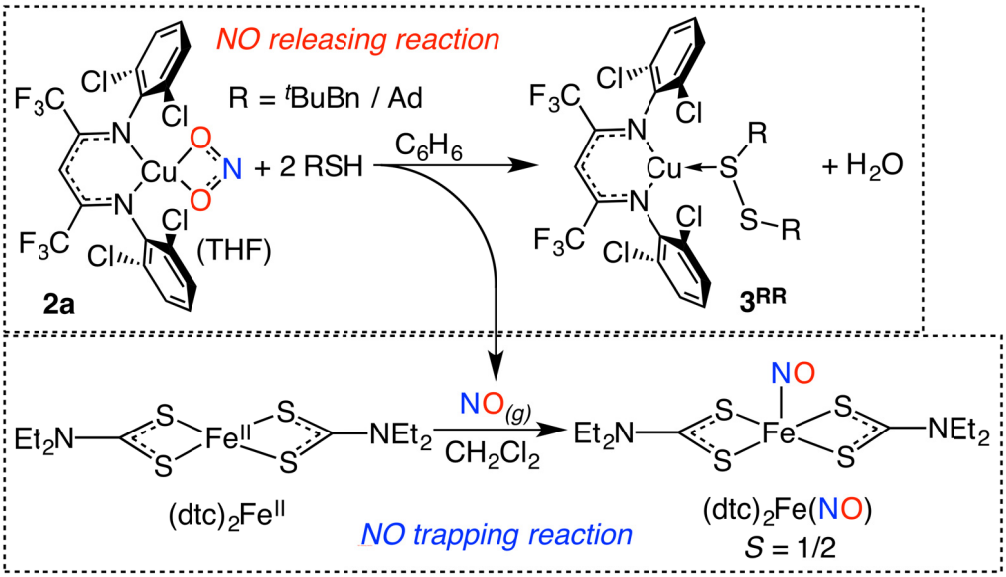

Figure S10. Stoichiometric conversion of $(dtc)_2Fe^{II}$ to $(dtc)_2Fe^{II}(NO)$ utilized for NO trapping.

$(dtc)_2Fe^{II}$ was employed for trapping of nitric oxide gas using a similar experimental setup as demonstrated in the previous section. A smaller vial charged with a solution of **2a** (1.0 mL 10.0 mM) in C_6H_6 was carefully placed in a larger vial containing a solution of $(dtc)_2Fe^{II}$ complex (10.0 mL, 1.0 mM) in CH_2Cl_2 and the bigger vial was sealed with a septum. A solution of 4-*tert*-butylbenzylthiol (^{t}BuBnSH) (1.0 mL 20.0 mM) in C_6H_6 was injected to the inner vial and the vials were gently shaken occasionally for 30 min. Then an aliquot (300 µL) of the resultant $(dtc)_2Fe$ solution from the outer vial was transferred to a quartz EPR tube and analyzed by X-band EPR spectroscopy. The room temperature EPR spectrum (Figure S11) exhibits a three line S = ½ signal at g_{iso} = 2.04 with $A(^{14}N)$ = 12.9 G, which is characteristic[7] of $(dtc)_2Fe(NO)$ complex.

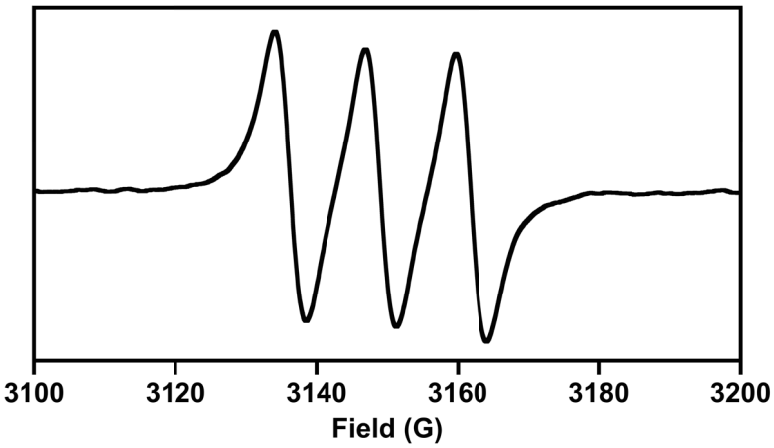

Figure S11. X-band EPR spectrum (1.0 mM in CH_2Cl_2 at 25 °C) of [$(dtc)_2Fe(NO)$] species generated upon reacting $(dtc)_2Fe^{II}$ with $NO_{(g)}$ released from the mixture of **2a** and 4-*tert*-butylbenzylthiol (^{t}BuBnSH). Frequency = 8.9159230 GHz, Power 1 mW, Mod. Width = 0.01 mT, Time constant = 0.1 s.

8. Reaction of $[Cl_2NN_{F6}]Cu(\kappa^2\text{-}O_2N)$•THF (2a) with 1 equiv. 4-*tert*-butylbenzylthiol (^{t}BuBnSH).

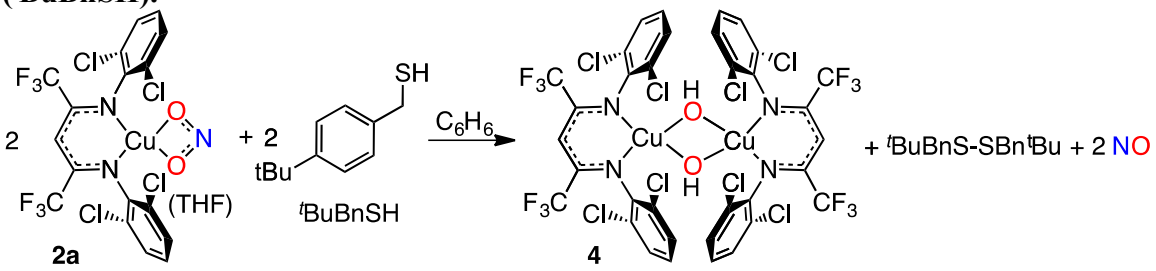

To a solution of **2a** (56.7 mg, 0.084 mmol) in C_6D_6 (0.5 mL), a solution of 4-*tert*-butylbenzylthiol (^{t}BuBnSH) (15.1 mg, 0.084 mmol, 15.6 μL) in C_6D_6 (0.5 mL) was added. The color of the solution immediately changed from dark green to yellow with concomitant formation of a brownish-yellow precipitate. After 10 min stirring, the resultant reaction mixture was filtered to separate the yellow solution and the brownish-yellow precipitate **4**. ^{1}H NMR analysis on the yellow solution exhibits the formation of free disulfide in near quantitative yield. ^{1}H NMR (400 MHz, 298 K, C_6D_6): δ 7.23 (d, 2H, *m*-Ar-*H*), 7.12 (d, 2H, *o*-Ar-*H*), 3.43 (s, 2H, *CH2*-Ar), 1.18 (s, 9H, ^{t}*Bu*-Ar).

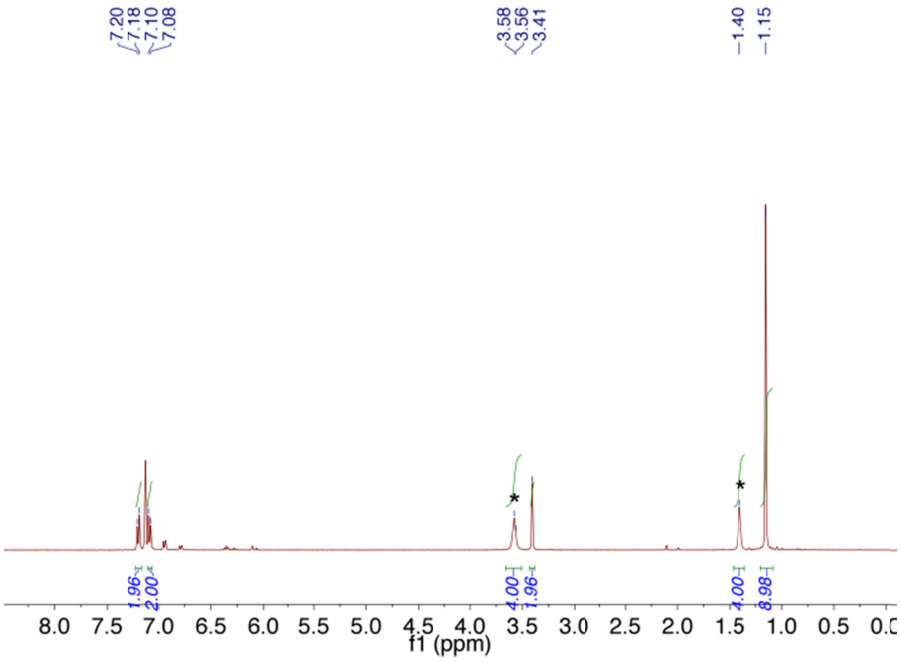

Figure S12. ^{1}H NMR spectrum (400 MHz, 298 K, C_6D_6) of the crude mixture obtained after filtration of the resultant reaction mixture consisting of **2a** and ^{t}BuBnSH (1 equiv). One equivalent of tetrahydrofuran (marked with *) originating from **2a** serves as internal standard and peaks are integrated relative to the four -C*H*$_2$O- type protons (from THF) at δ = 3.56 ppm, giving an NMR yield of 98% for the disulfide.

The brownish-yellow residue **4** after the filtration was washed thoroughly with pentane and dried under vacuum. FT-IR spectra of **4** (see Figure S13) shows a sharp vibrational band at 3652 cm^{-1} diagnostic of a bis(μ-hydroxo)dicopper(II) species. Gravimetric analysis gave the yield to be 41.2 mg, 0.035 mmol, 85%. Slow evaporation of a saturated fluorobenzene solution of **4** led to grow X-ray quality crystals. The molecular structure of **4** (see Figure S29) determined by X-ray crystallography indeed confirms the presence of the bis(μ-hydroxo)dicopper(II) core in **4**. Anal. calcd. for $C_{34}H_{16}F_{12}N_4O_2Cl_4Cu_2$: C, 35.47; H, 1.40; N, 4.87. Found: C, 35.72; H, 1.63; N, 4.81.

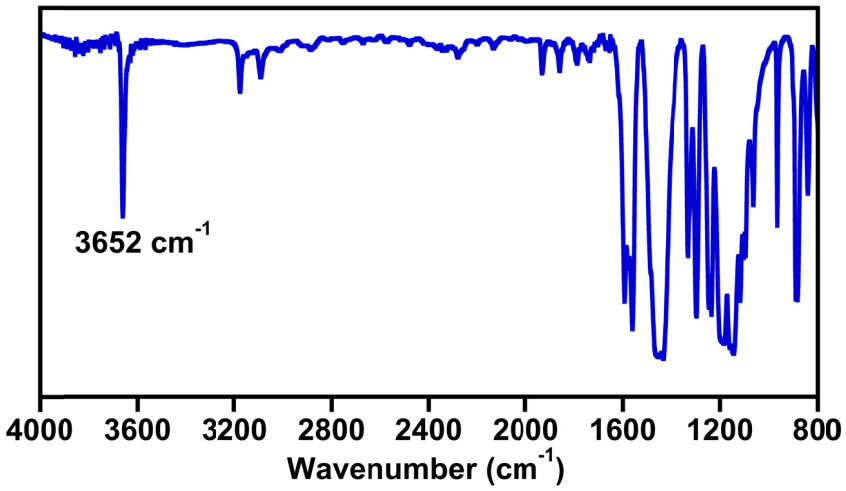

Figure S13. FT-IR spectrum (KBr pellet) of the brownish yellow residue **4** obtained from the reaction of **2a** with one equivalents of 4-*tert*-butylbenzylthiol (^{t}BuBnSH). FT-IR of **4** (KBr pellet): ν_{OH} 3652 cm^{-1}.

9. Reaction of $[Cl_2NN_{F6}]Cu(\kappa^2\text{-}O_2N)$•THF (2a) with 1 equiv. 1-adamantylthiol (AdSH).

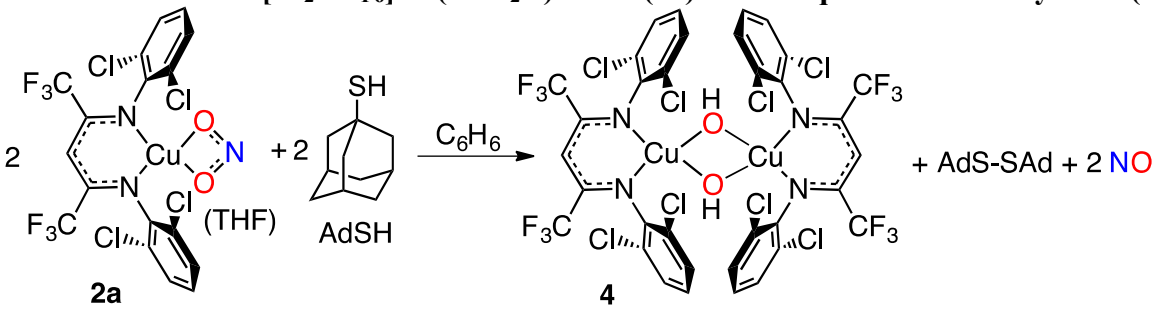

To a solution of $[Cl_2NN_{F6}]Cu(\kappa^2\text{-}O_2N)$•THF (**2a**) (59.3 mg, 0.087 mmol) in C_6D_6 (0.5 mL), a solution of 1-adamantylthiol (AdSH) (14.7 mg, 0.087 mmol) in C_6D_6 (0.5 mL) was added. The color of the solution immediately changed from dark green to greenish-yellow with concomitant formation of a brownish-yellow precipitate. After 30 min stirring, the resultant reaction mixture was filtered to isolate the yellowish solution and the brownish-yellow precipitate **4**. ^{1}H NMR analysis on the yellow solution indicates the formation of free disulfide in near quantitative yield. ^{1}H NMR (400 MHz, 298 K, C_6D_6): δ 1.93 (br, 12H, *CH*-Ad), 1.87 (br, 6H, CH_2-Ad), 1.50 (br, 12H, CH_2-Ad).

The brownish-yellow residue **4** after the filtration was washed thoroughly with pentane and dried under vacuum. Gravimetric analysis gave the yield to be 42.1 mg, 0.036 mmol, 84%).

10. Reaction of $[Cl_2NN_{F6}]Cu(\kappa^2\text{-}O_2N)$•THF (2a) with 1 equiv. tritylthiol (Ph_3CSH).

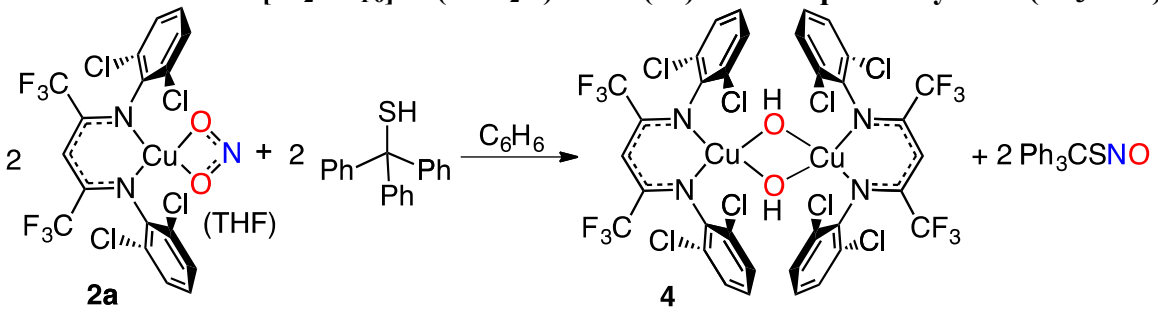

To a solution of $[Cl_2NN_{F6}]Cu(\kappa^2\text{-}O_2N)$•THF (**2a**) (54.1 mg, 0.079 mmol) in C_6D_6 (0.5 mL), a solution of tritylthiol (Ph_3CSH) (22.1 mg, 0.079 mmol) in C_6D_6 (0.4 mL) was added. The color of the solution immediately changed from dark green to light greenish brown with simultaneous formation of a brownish-yellow precipitate. After 30 min stirring, the resultant reaction mixture was filtered to isolate the light green solution and the brownish-yellow precipitate **4**. UV-vis spectroscopic analysis (see Figure S14) on the light green solution shows a band at 600 nm, which is characteristic of Ph_3CSNO.[8]

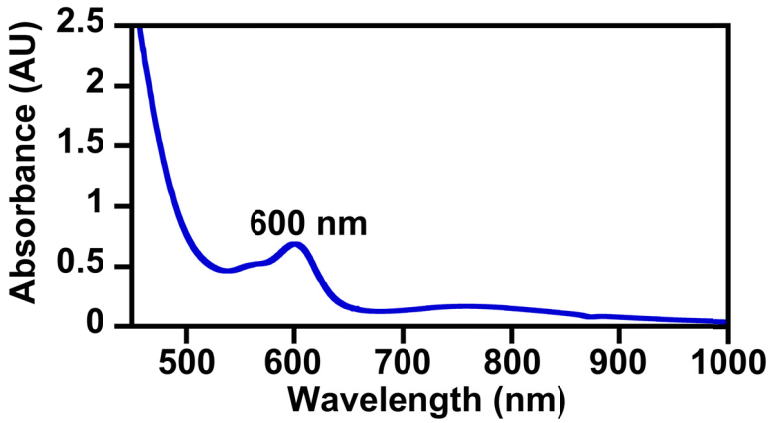

Figure S14. UV-vis spectrum (33.0 mM in benzene at 25 °C) of the green filtrate obtained from the reaction of **2a** with one equivalents of Ph_3CSH. The spectroscopic yield of Ph_3CSNO was estimated on the basis of its molar extinction coefficient (ε = 22 $M^{-1}cm^{-1}$) for λ_{max} = 600 nm obtained from the Beer's plot of an authentic sample of Ph_3CSNO in benzene at 25 °C.

11. Reaction of $[Cl_2NN_{F6}]Cu(\kappa^2\text{-}O_2N)$•THF (2a) with *tert*-Butanol.

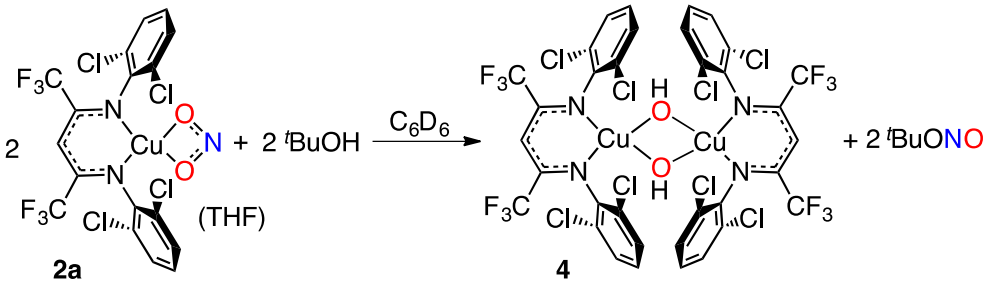

A solution of $[Cl_2NN_{F6}]Cu(\kappa^2\text{-}O_2N)$•THF (**2a**) (0.088 g, 0.130 mmol) in C_6D_6 (1.0 mL) was treated with 12.2 μL of *tert*-butanol (0.130 mmol) and the reaction mixture was stirred for 8 h. The color of the resultant reaction mixture turned very faint green with concomitant formation of a brownish precipitate. The reaction mixture was filtered to isolate the brownish-yellow precipitate of **4** (0.053 g, 0.046 mmol) in 71% yield. The filtrate was analyzed by ^{1}H NMR spectroscopy which showed the formation of ^{t}BuONO in 45% yield.

The addition of *tert*-butanol in excess accelerates the formation of ^{t}BuONO and results in a higher yield. A solution of $[Cl_2NN_{F6}]Cu(\kappa^2\text{-}O_2N)$•THF (**2a**) (0.042 g, 0.062 mmol) in C_6D_6 (1.0 mL) was treated with 20 equiv. *tert*-butanol (118.2 μL, 1.237 mmol) and the reaction mixture was stirred for 4 h. After filtration, the filtrate was analyzed by ^{1}H NMR spectroscopy which showed the formation of ^{t}BuONO in 61% yield.

While we have not performed any independent reactions of ^{t}BuONO with any of the copper complexes pertinent to this study, ^{t}BuONO is known to undergo ^{t}BuO-NO cleavage with an electron-rich copper(I) β-diketiminate.[9]

The formation of ^{t}BuONO was further confirmed by ^{15}N NMR spectroscopy. A ^{15}N enriched sample was prepared by addition of 24 μL of *tert*-butanol (0.258 mmol) to a solution of [Cl_2NN_{F6}]Cu(κ^2-O_2^{15}N)•THF (**2a**-^{15}N) (0.031 g, 0.046 mmol) in C_6D_6 (0.5 mL).

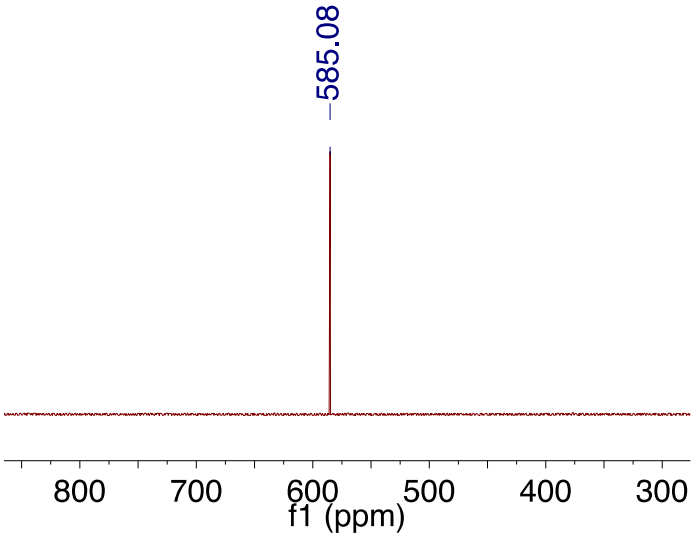

Figure S15. ^{15}N NMR spectrum (41 MHz, 298 K, C_6D_6) of the crude mixture obtained after filtration of the reaction mixture consisting of **2a**-^{15}N and ^{t}BuOH. The ^{15}N resonance is externally referenced to Na$^{15}NO_2$ in D_2O (609.5 ppm *vs* liquid NH_3) and was compared with authentic sample of ^{15}N enriched ^{t}BuO^{15}NO.

12. Reaction of $[Cl_2NN_{F6}]Cu(\kappa^2\text{-}O_2N)$•THF (2a) with diphenylamine (Ph_2NH).

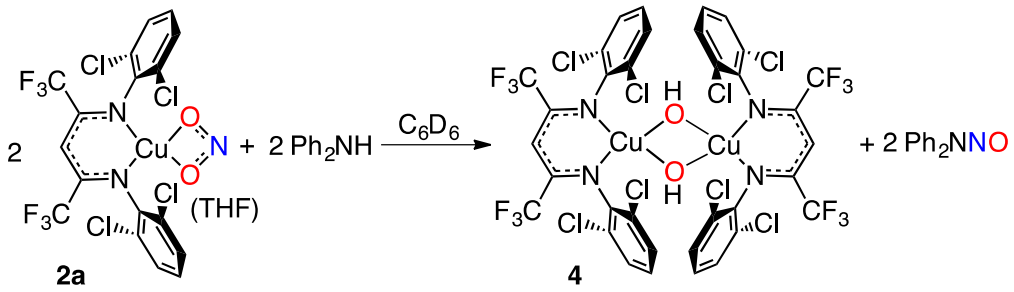

A solution of $[Cl_2NN_{F6}]Cu(\kappa^2\text{-}O_2N)$•THF (**2a**) (0.050 g, 0.074 mmol) in C_6D_6 (0.8 mL) was treated with diphenylamine (0.013 g, 0.074 mmol) and the reaction mixture was stirred for 8 h. The color of the resultant reaction mixture turned yellowish with concomitant formation of a brownish precipitate. The reaction mixture was filtered to isolate the brownish-yellow precipitate of **4** (0.032 g, 0.028 mmol) in 75% yield. The filtrate was analyzed by ^{1}H NMR spectroscopy which showed the formation of Ph_2NNO in 58% yield.

The addition of diphenylamine in excess accelerates the formation of Ph_2NNO and results in a higher yield. A solution of $[Cl_2NN_{F6}]Cu(\kappa^2\text{-}O_2N)$•THF (**2a**) (0.027 g, 0.004 mmol) in C_6D_6 (1.0 mL) was treated with 10 equiv. diphenylamine (0.068 g, 0.040 mmol) and the reaction mixture was stirred for 2 h. After filtration, the filtrate was analyzed by ^{1}H NMR spectroscopy which showed the formation of Ph_2NNO in 74% yield.

While we have not performed any independent reactions of Ph_2NNO with any of the copper complexes pertinent to this study, Ph_2NNO is known to undergo Ph_2N-NO cleavage with a more electron-rich copper(I) β-diketiminate.[10]

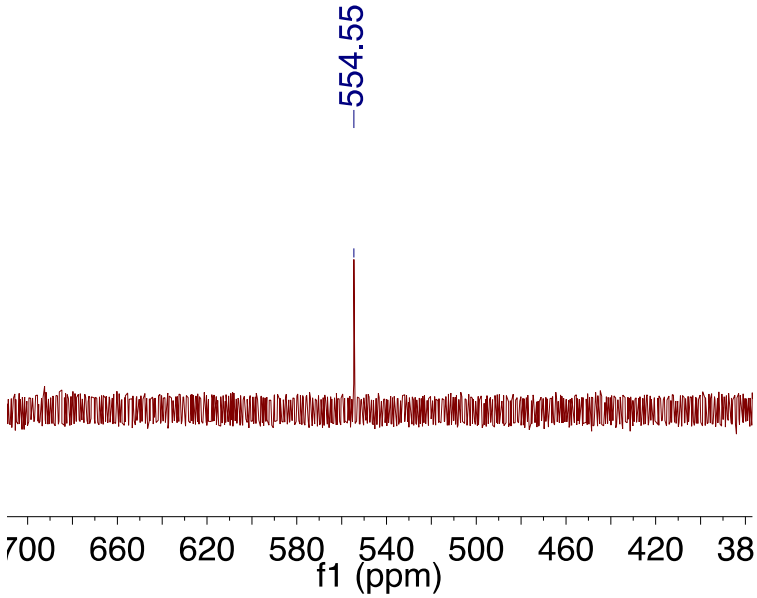

Figure S16. ^{15}N NMR spectrum (41 MHz, 298 K, C_6D_6) of the crude mixture obtained after filtration of the reaction mixture consisting of **2a**-^{15}N and Ph_2NH (1 equiv). The ^{15}N resonance is externally referenced to $Na^{15}NO_2$ in D_2O (609.5 ppm *vs* liquid NH_3) and was compared with authentic sample of ^{15}N enriched $Ph_2N^{15}NO$.

13. Reaction of {[Cl_2NN_{F6}]Cu}$_2$(μ-OH)$_2$ (4) with trityl thiol (Ph_3CSH).

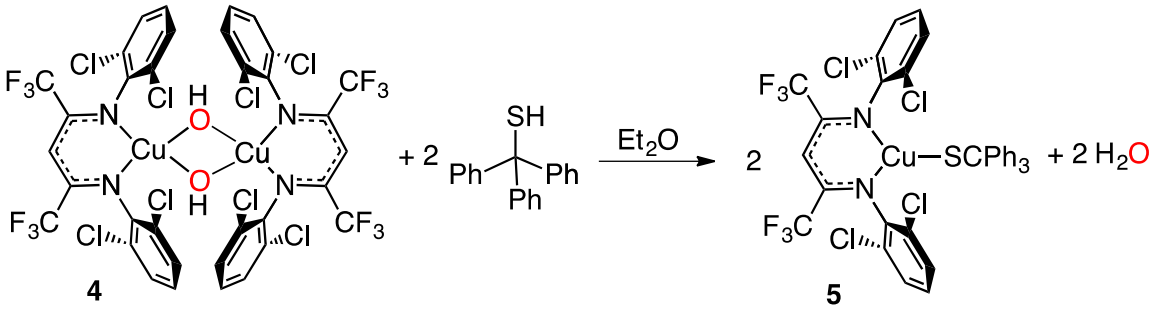

A solution of {[Cl_2NN_{F6}]Cu}$_2$(μ-OH)$_2$ (**4**) in Et_2O (2.0 mL, 0.25 mM) was taken in a quartz cuvette sealed with a septum. A solution of Ph_3CSH in Et_2O (0.1 mL, 10.0 mM) was injected to the previous solution and the progress of the reaction was monitored by UV-vis spectroscopy. A new band centered at 760 nm started to develop at room temperature (Figure S17). Charge transfer bands around 700-800 nm were previously reported to be characteristic of β-diketiminate copper(II) thiolate complexes such as [Me_2NN]Cu-$SCPh_3$ (λ = 731 nm)[9] and [^{i}Pr_2NN]Cu-$SCPh_3$ (λ = 749 nm)[11]. An independent synthesis of [Cl_2NN_{F6}]Cu-$SCPh_3$ (**5**) was attempted to confirm this assignment (see Section 15).

Note: The 760 nm species is unstable at 25 °C; however, the reaction that forms this species is very slow at lower temperatures (-40 to 0 °C).

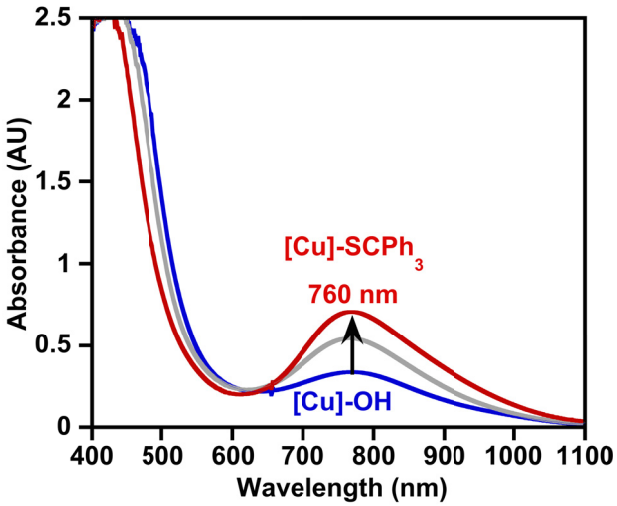

Figure S17. Changes in the UV-vis spectrum of {[Cl_2NN_{F6}]Cu}$_2$(μ-OH)$_2$ (**4**) (0.25 mM in diethyl ether at 25 °C) (blue trace) upon addition of two equivalents of Ph_3CSH.

14. Synthesis and Characterization of $[Cl_2NN_{F6}]Cu\text{-}O^tBu$ (6).

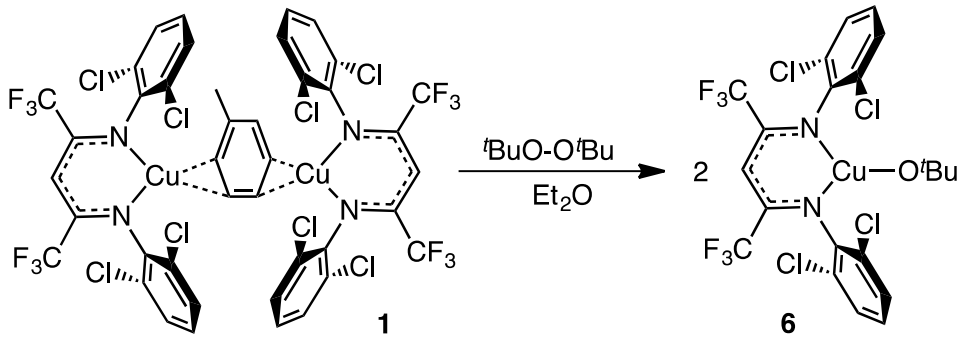

$[Cl_2NN_{F6}]Cu\text{-}O^tBu$ (**6**) was prepared by slight modification of a previously reported procedure.[12] A solution of di-*tert*-butyl peroxide ($^tBuOO^tBu$) (300 μL, 1.620 mmol) in Et_2O (1.0 mL) was added dropwise to a chilled suspension of **1** (0.412 g, 0.341 mmol) in Et_2O (5 mL) and the color of the reaction mixture immediately turned dark reddish-purple. The reaction mixture was stirred at room temperature for 1 h and filtered through celite. A dark purple filtrate was concentrated under reduced pressure and left at -40 °C. The dark brownish crystals thus obtained were decanted from the mother liquor and dried under vacuum to afford a brownish powder of the desired product **6** (0.326 g, 0.516 mmol) in 76% yield. Anal. calcd. for $C_{21}H_{16}F_6N_2OCl_4Cu$: C, 39.93; H, 2.55; N, 4.43. Found: C, 39.98; H, 2.57; N, 4.32. UV-Vis (Pentane, 25 °C): λ_{max} = 510 nm (ε = 2360 $M^{-1}cm^{-1}$) (Figure S18). X-band EPR (Pentane, 293 K): g_{iso} = 2.111, A_{iso}(Cu) = 110.0 MHz, A_{iso}(2N) = 32.0 MHz (Figure S22). X-band EPR (Pentane, 80 K): g_1 = 2.210, g_2 = 2.089, g_3 = 2.034, A_1(Cu) = 350 MHz, A_2(Cu) = 5 MHz, A_3(Cu) = 5 MHz, A_1(2N) = A_2(2N) = A_3(2N) = 35 MHz (Figure S23).

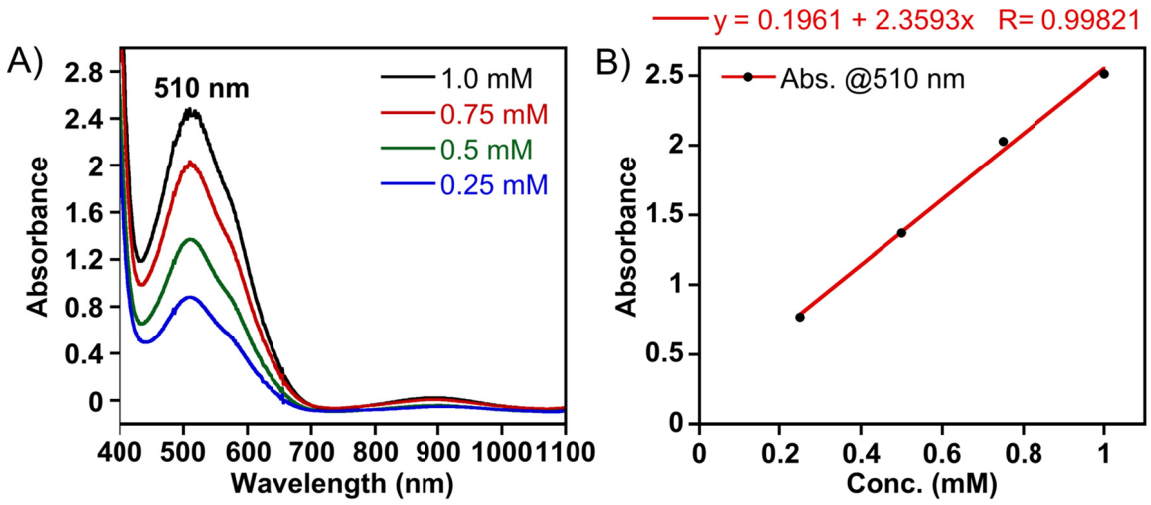

Figure S18. (A) UV-Vis spectra of $[Cl_2NN_{F6}]$Cu-O^{t}Bu (**6**) in pentane at 25 °C at different concentrations. (B) Beer's law plot for **6** depicts λ_{max}/nm (ε/M^{-1}cm^{-1}) = 510 (2360).

15. Reaction of $[Cl_2NN_{F6}]Cu\text{-}O^tBu$ (6) with 1 equiv. trityl thiol (Ph_3CSH).

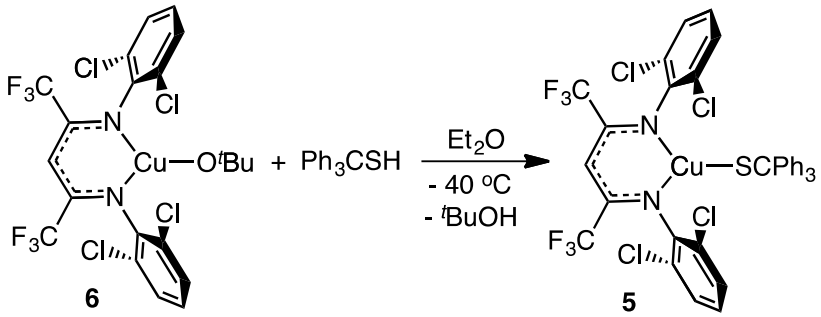

A solution of $[Cl_2NN_{F6}]Cu\text{-}O^tBu$ (**6**) in Et_2O (2.0 mL, 0.25 mM) was taken in a quartz cuvette capped with a septum. A solution of Ph_3CSH in Et_2O (0.1 mL, 5.0 mM) was injected to the previous solution at -40 °C and the progress of the reaction was followed by UV-vis spectroscopy. A new optical band centered at 760 nm started to develop with simultaneous decay of the absorption feature of **6** at 510 nm. We assign the 760 nm band as the charge transfer band of copper(II) thiolate **5**.

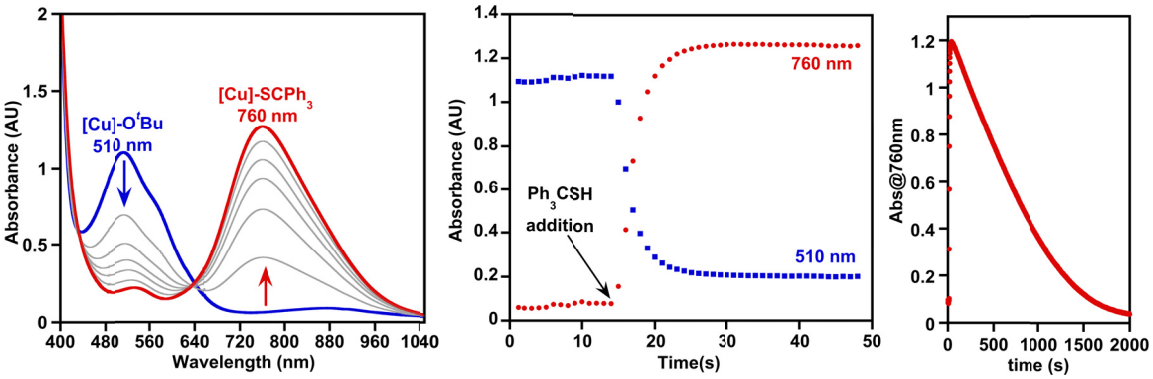

Figure S19. UV-Vis spectral changes (left) and time traces (middle and right) in diethyl ether at -40 °C. Left: Changes in the UV-vis spectrum of $[Cl_2NN_{F6}]Cu\text{-}O^tBu$ (**6**) (0.25 mM (blue trace) upon addition of one equivalents of Ph_3CSH. Middle: Time traces shows the $[Cu^{II}]\text{-}O^tBu$ (**6**) to $[Cu^{II}]\text{-}SCPh_3$ (**5**) transformation. Right: Decay of the 760 nm band over longer period of time at -40 °C.

*Note: The $[Cl_2NN_{F6}]Cu^{II}\text{-}SCPh_3$ (**5**) species is not stable at -40 °C which hampered its detailed characterization; however, closely related β-diketiminato copper(II)-thiolate complexes have been previously structurally and spectroscopically characterized.*[9,11]

16. Reaction of $[Cl_2NN_{F6}]$Cu-SCPh$_3$ (5) with 1 equiv. 1-adamantyl *S*-nitrosothiol (AdSNO).

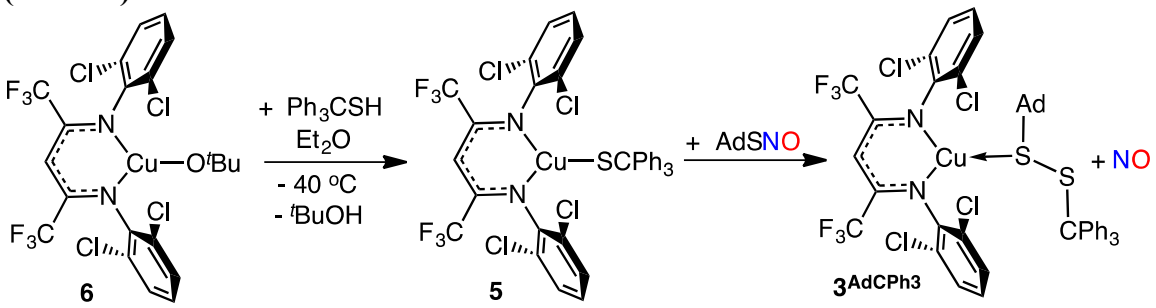

A solution of Ph_3CSH (0.042 g, 0.152 mmol) in Et_2O (0.5 mL) was added to a dark reddish-purple solution of $[Cl_2NN_{F6}]$Cu-O^{t}Bu (**6**) (0.096 g, 0.152 mmol) in Et_2O (3 mL) at -40 °C to generate $[Cl_2NN_{F6}]$Cu-SCPh$_3$ (**5**). After stirring for a minute, a solution of AdSNO (0.030 g, 0.152 mmol) in Et_2O (0.5 mL) was added to the *in situ* generated copper(II) thiolate **5** and the color of the resultant reaction mixture immediately turned dark orange. The solvent was evaporated to obtain an orange sticky mass, which was redissolved in pentane and left at -40 °C. X-ray quality crystals of **3**$^{\mathbf{AdCPh3}}$ were grown from the pentane solution after few days. The poor yield of **3**$^{\mathbf{AdCPh3}}$ hindered isolation and detailed characterization of the complex. The X-ray crystal structure of **3**$^{\mathbf{AdCPh3}}$, however, demonstrates the possible generation of the mixed disulfide from $[Cl_2NN_{F6}]$Cu-SCPh$_3$ and AdSNO (Figure S31).

Formation of NO from the reaction of $[Cl_2NN_{F6}]$Cu-SCPh$_3$ (**5**) and AdSNO was qualitatively confirmed by employing (dtc)$_2$Fe^{II} complex as a NO trap. See pages S13-S14 for representative experimental details.

17. X-Band EPR Spectra of $[Cl_2NN_{F6}]Cu(\kappa^2\text{-}O_2N)\bullet THF$ (2a), $[Cl_2NN_{F6}]Cu\text{-}OtBu$ (6), and $[Cl_2NN_{F6}]Cu\text{-}SCPh_3$ (5).

General considerations. EPR spectra were collected on a JEOL continuous wave spectrometer JES-FA200 equipped with an X-band Gunn oscillator bridge, a cylindrical mode cavity, and a liquid nitrogen cryostat. EPR measurements were performed in sealed quartz tubes.

All spectra were obtained on freshly prepared solutions (0.5 - 2 mM in pentane) of at least two independently synthesized batches and were checked carefully for reproducibility. Background spectra were obtained on clean solvents at the same measurement conditions.

Spectral simulation was performed using the program QCMP 136 by Prof. Dr. Frank Neese from the Quantum Chemistry Program Exchange as used by Neese *et al.* in *J. Am. Chem. Soc.* **1996**, *118*, 8692-8699. The fittings were performed by the "chi by eye" approach and always taking all available spectra at different temperatures into account. Collinear g and A tensors were used. Spectral simulations were performed using the simple 1 Cu, 2 N model (nuclear spin for $^{63/65}$Cu: $I = 3/2$ and for ^{14}N: $I = 1$). The A(N) values used are only estimates and contribute line broadening since resolved hyperfine to ^{14}N is not explicitly observed in the EPR spectra of **2a**, **5**, and **6**.

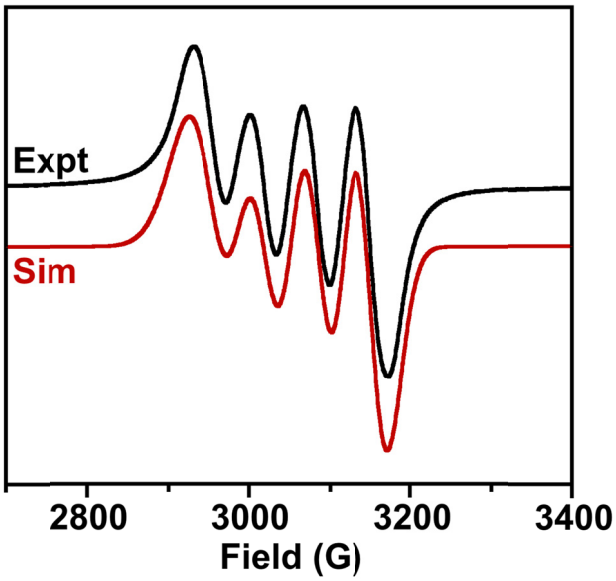

Figure S20. X-band EPR spectrum (black trace) and simulation (red trace) of $[Cl_2NN_{F6}]Cu(\kappa^2\text{-}O_2N)$•THF (**2a**) (pentane, 293 K, Frequency = 8.9527 GHz, Power = 0.99 mW, ModWidth = 0.4 mT, time constant = 0.1 s). Simulation was performed using 1Cu, 2N model: g_{iso} = 2.106, A_{iso}(Cu) = 189.0 MHz, A_{iso}(2N) = 29.0 MHz, Gaussian line shape with line broadening of W_{iso} = 26.4 mT.

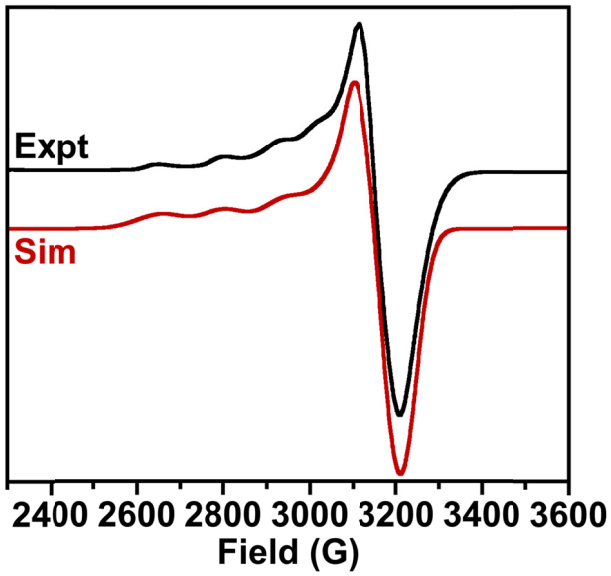

Figure S21. X-band EPR spectrum (black trace) and simulation (red trace) of $[Cl_2NN_{F6}]Cu(\kappa^2\text{-}O_2N)$•THF (**2a**) (pentane, 80 K, Frequency = 8.9993 GHz, Power = 0.99 mW, ModWidth = 1.0 mT, time constant = 0.3 s). Simulation was performed using 1Cu, 2N model: g_1 = 2.244, g_2 = 2.036, g_3 = 2.036, A_1(Cu) = 440 MHz, A_2(Cu) = 70 MHz, A_3(Cu) = 20 MHz, A_1(2N) = A_2(2N) = A_3(2N) = 29 MHz, Gaussian line shape with line broadening of W_1 = 60 mT, W_2 = W_3 = 28 mT.

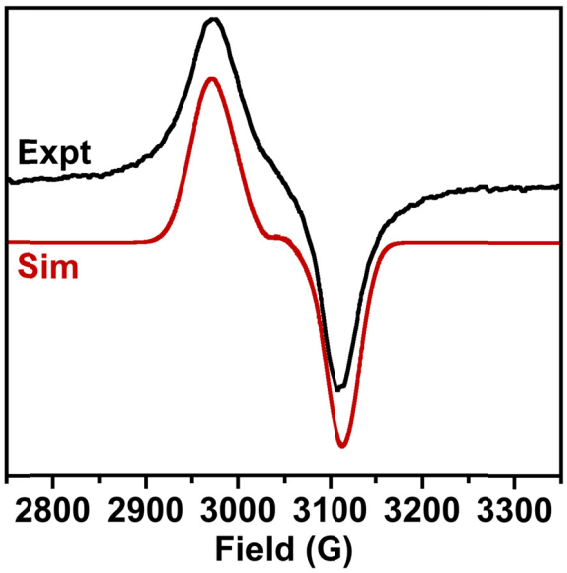

Figure S22. X-band EPR spectrum (black trace) and simulation (red trace) of $[Cl_2NN_{F6}]$Cu-O^{t}Bu (**6**) (pentane, 293 K, Frequency = 8.9745 GHz, Power = 0.99 mW, ModWidth = 1.0 mT, time constant = 0.03 s). Simulation was performed using 1Cu, 2N model: g_{iso} = 2.111, A_{iso}(Cu) = 110.0 MHz, A_{iso}(2N) = 32.0 MHz, Gaussian line shape with line broadening of W_{iso} = 22.0 mT.

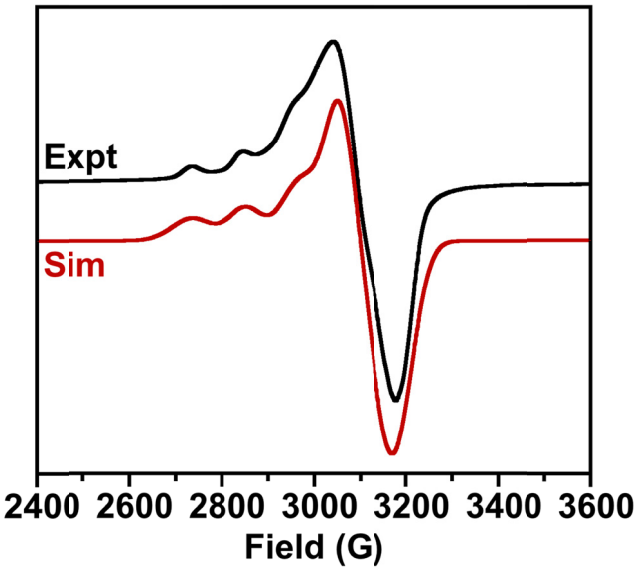

Figure S23. X-band EPR spectrum (black trace) and simulation (red trace) of $[Cl_2NN_{F6}]$Cu-O^{t}Bu (**6**) (pentane, 80 K, Frequency = 8.9935 GHz, Power = 0.99 mW, ModWidth = 1.0 mT, time constant = 0.1 s). Simulation was performed using 1Cu, 2N model: g_1 = 2.210, g_2 = 2.089, g_3 = 2.034, A_1(Cu) = 350 MHz, A_2(Cu) = 5 MHz, A_3(Cu) = 5 MHz, A_1(2N) = A_2(2N) = A_3(2N) = 35 MHz, Gaussian line shape with line broadening of W_1 = 40.5 mT, W_2 = 27.5 mT, W_3 = 32.5 mT.

The room temperature EPR spectrum of **5** is not reported due to thermal sensitivity of **5**.

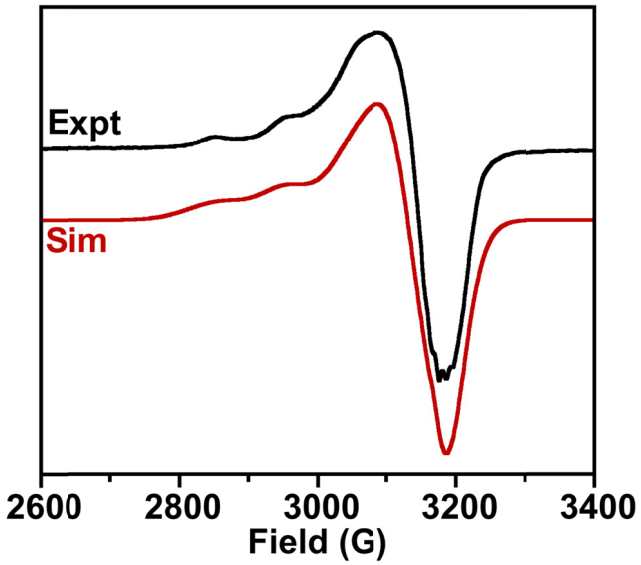

Figure S24. X-band EPR spectrum (black trace) and simulation (red trace) of $[Cl_2NN_{F6}]Cu$-$SCPh_3$ (**5**) (pentane, 80 K, Frequency = 8.9945 GHz, Power = 0.99 mW, ModWidth = 1.0 mT, time constant = 0.1 s). Simulation was performed using 1Cu, 2N model: g_1 = 2.142, g_2 = 2.067, g_3 = 2.035, A_1(Cu) = 280 MHz, A_2(Cu) = 5 MHz, A_3(Cu) = 5 MHz, A_1(2N) = A_2(2N) = A_3(2N) = 32 MHz, Gaussian line shape with line broadening of W_1 = 38.4 mT, W_2 = W_3 = 28.4 mT.

18. Crystallographic details and additional structures.

Single crystals of each compound **2** (CCDC 1513099), **2a** (CCDC 1513100), $\mathbf{3^{BnBn}}$ (CCDC 1513101)**,** $\mathbf{3^{AdAd}}$ (CCDC 1513102), **4** (CCDC 1513104), $\mathbf{3^{AdCPh3}}$ (CCDC 1513103), and **6** (CCDC 1513105) were mounted under mineral oil on Mitegen micro mounts and immediately placed in a cold nitrogen stream at 100(2) K. Data for compounds **2**, **2a**, $\mathbf{3^{BnBn}}$, $\mathbf{3^{AdCPh3}}$, and **6** were collected on a Bruker D8 Quest equipped with a Photon100 CMOS detector and a MoImS source. Data for compounds **4** and $\mathbf{3^{AdAd}}$ were collected on a Bruker DUO equipped with an APEXII CCD detector and Mo fine focus sealed tube source. Either full spheres (triclinic) or hemispheres (monoclinic or higher) of data were collected (0.3° or 0.5° ω-scans; $2\theta_{max} = 56$ °; monochromatic Mo Kα radiation, $\lambda = 0.7107$ Å) depending on the crystal system and integrated with the Bruker SAINT program. Structure solutions were performed using the SHELXTL/PC suite[13] and XSEED.[14] Intensities were corrected for Lorentz and polarization effects and an empirical absorption correction was applied using Blessing's method as incorporated into the program SADABS.[15] Non-hydrogen atoms were refined with aniostropic thermal parameters and hydrogen atoms were included in idealized positions. Structures were rendered with POV-Ray in XSEED using 50% probability ellipsoids.

Further comments on disorder models:

$[Cl_2NN_{F6}]$Cu(^{t}BuBnS-SBn^{t}Bu) ($\mathbf{3^{BnBn}}$). One CF_3 group is disordered over two positions. The like C-F distances were restrained to be similar (esd 0.01Å).

$[Cl_2NN_{F6}]$Cu(AdS-SAd) ($\mathbf{3^{AdAd}}$). The datum crystal was twinned. The secondary domain is related to the primary domain by the twin law (1 0 0), (0 -1 0), (-1 0 -1). The relative ratio of the domains refines to 61% : 39%. The disulfide ligand is disordered over two positions. The like Cu-S, S-C, and C-C distances were restrained to be similar (esd 0.01Å).

$[Cl_2NN_{F6}]$Cu-O^{t}Bu (6). The methyl groups of the t-butyl moiety are disordered across a mirror plane. These atoms were treated with a negative PART command and their site occupancies were fixed to 0.5. The like C-C distances were restrained to be similar (esd 0.01Å).

$[Cl_2NN_{F6}]$Cu(AdS-SCPh$_3$) ($\mathbf{3^{AdCPh3}}$). One of the CF_3 groups is disordered over three positions. The like C-F distances were restrained to be similar (esd 0.01Å).

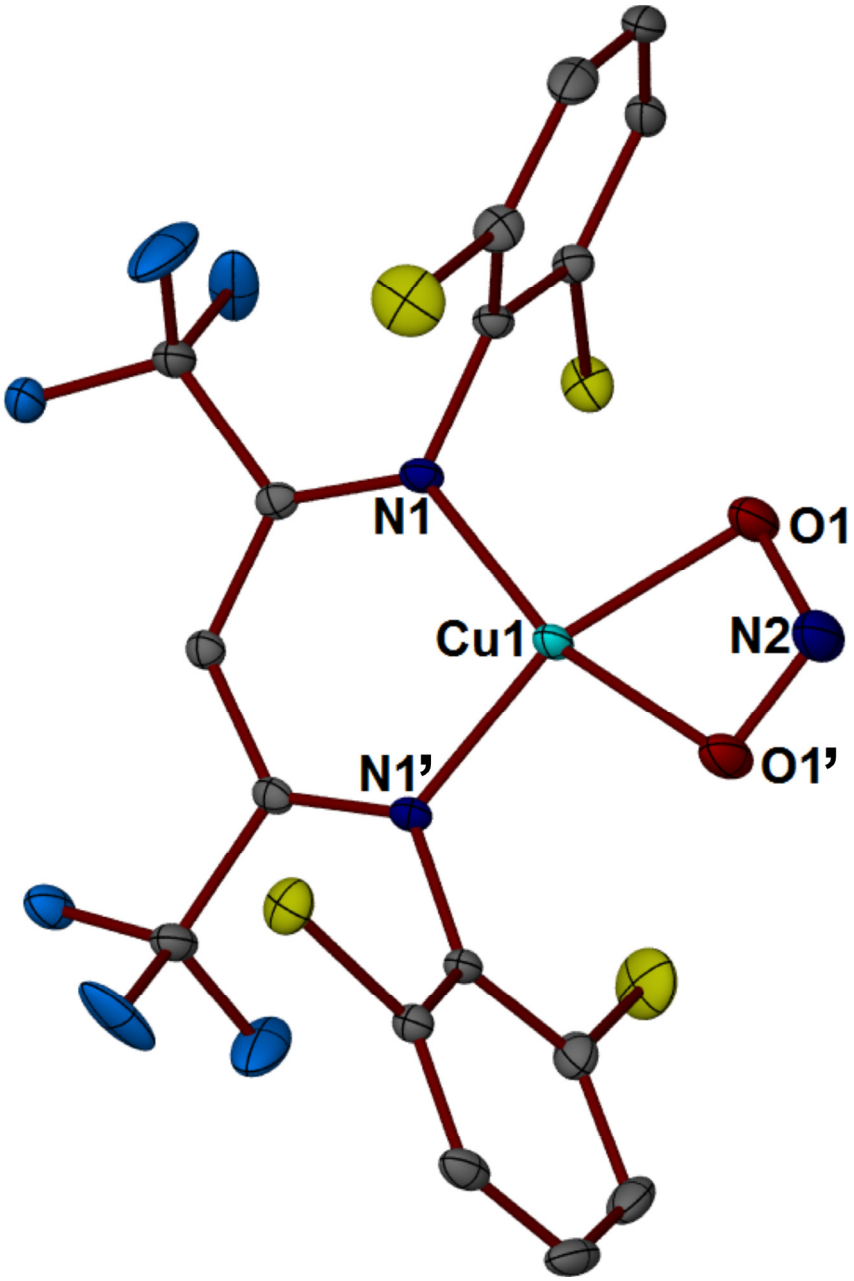

Figure S25. Molecular structure of $[Cl_2NN_{F6}]Cu(\kappa^2\text{-}O_2N)$ (**2**) (CCDC 1513099). The thermal ellipsoid plots are drawn at 50% probability level. N1' and O1' are symmetry generated atoms. Hydrogen atoms are omitted for clarity. Selected bond distances (Å) and angles (°): Cu1-N1 1.9092(13), Cu1-N1' 1.9091(13), Cu1-O1 2.0140(12), Cu1-O1' 2.0140(12), O1-N2 1.2693(17), O1'-N2 1.2693(17), N1-Cu1-N1' 96.85(8), N1-Cu1-O1 100.83(5), N1'-Cu1-O1' 100.84(5), O1-N2-O1' 110.3(2).

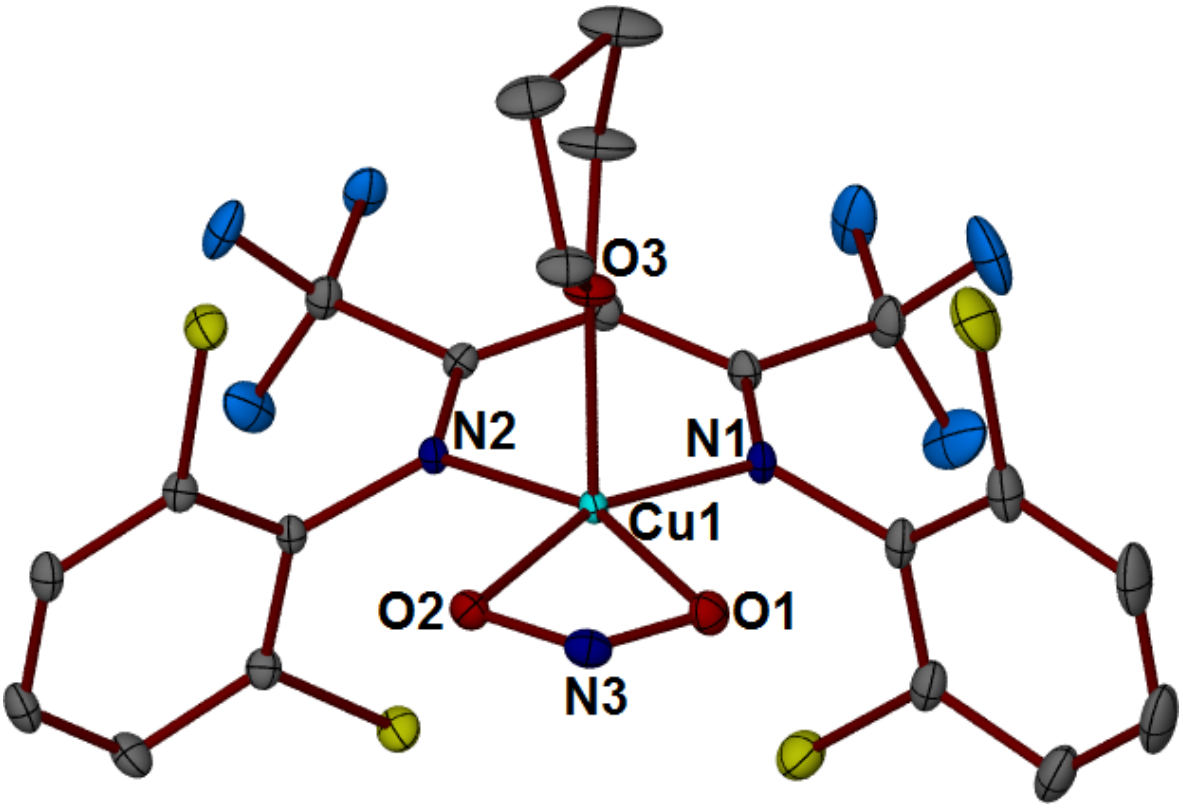

Figure S26. Molecular structure of $[Cl_2NN_{F6}]Cu(\kappa^2\text{-}O_2N)$•THF (**2a**) (CCDC 1513100). The thermal ellipsoid plots are drawn at 50% probability level. Hydrogen atoms are omitted for clarity. Selected bond distances (Å) and angles (°): Cu1-N1 1.9421(9), Cu1-N2 1.9398(9), Cu1-O1 2.0350(8), Cu1-O2 2.0335(8), Cu1-O3 2.1922(8), O1-N3 1.2641(13), O2-N3 1.2723(13), N1-Cu1-N2 94.91(4), N1-Cu1-O1 100.47(4), N2-Cu1-O2 101.23(4), O1-Cu1-O2 61.67(3), O1-N3-O2 110.60(9).

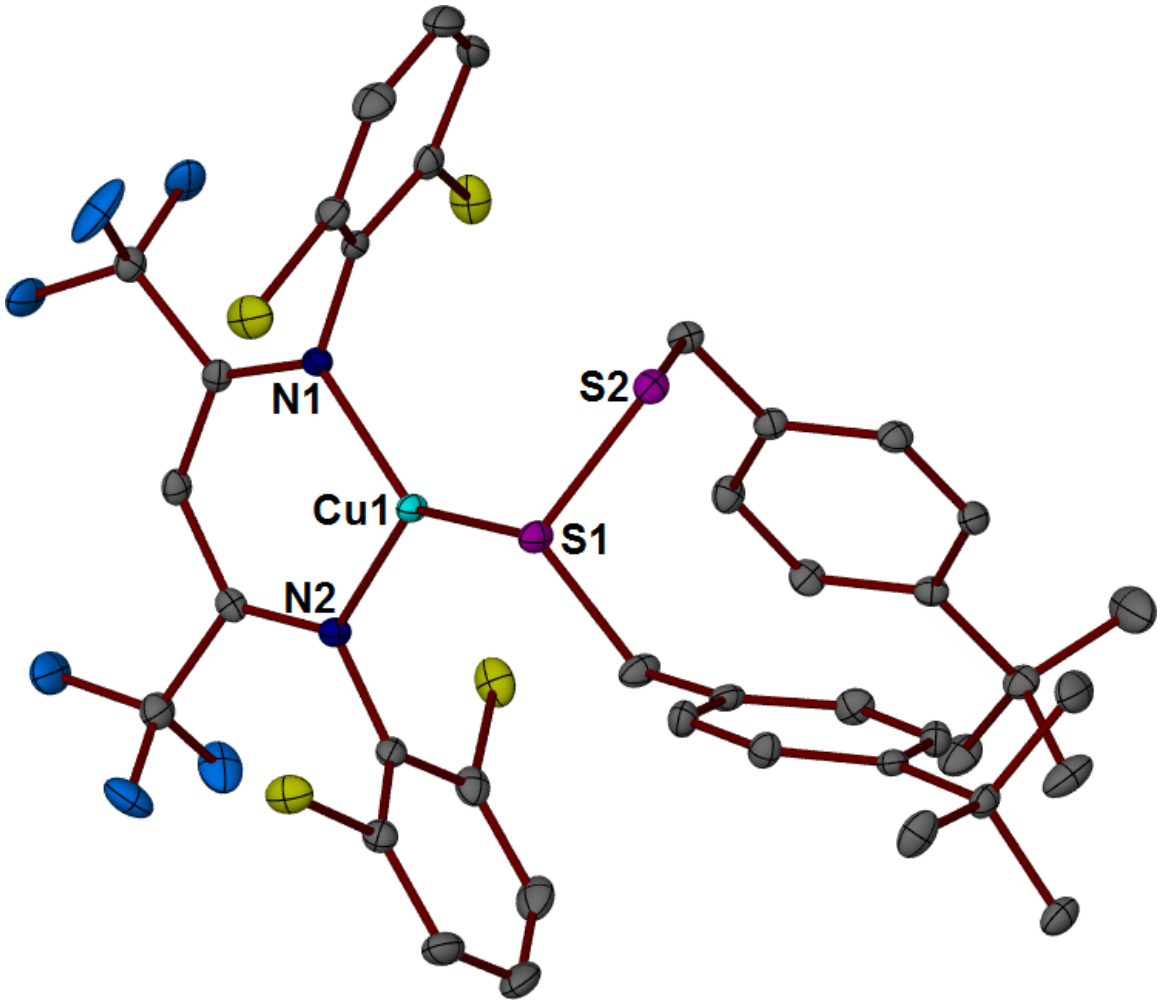

Figure S27. Molecular structure of $[Cl_2NN_{F6}]Cu(^t$BuBnS-SBn^{t}Bu) (**3**$^{\mathbf{BnBn}}$) (CCDC 1513101). The thermal ellipsoid plots are drawn at 50% probability level. Hydrogen atoms are omitted for clarity. Only the major component of disordered sites is shown. Selected bond distances (Å) and angles (°): Cu1-N1 1.9473(13), Cu1-N2 1.9436(13), Cu1-S1 2.1614(4), S1-S2 2.0477(6), N1-Cu1-N2 99.39(5), N1-Cu1-S1 130.86(4), N2-Cu1-S1 128.52(4).

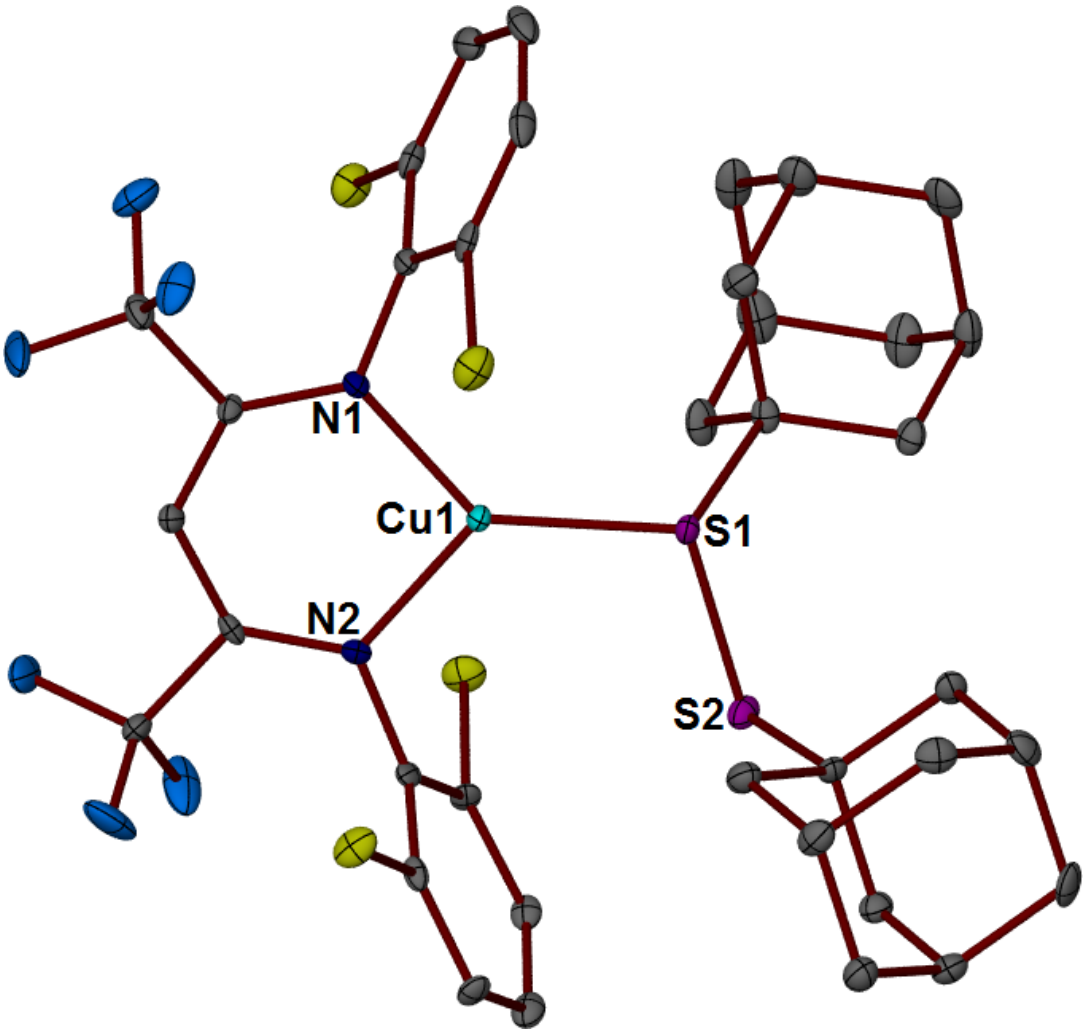

Figure S28. Molecular structure of $[Cl_2NN_{F6}]Cu(AdS\text{-}SAd)$ (**3**^{AdAd}) (CCDC 1513102). The thermal ellipsoid plots are drawn at 50% probability level. Hydrogen atoms are omitted for clarity. Only the major component of disordered sites is shown. Selected bond distances (Å) and angles (°): Cu1-N1 1.945(5), Cu1-N2 1.969(5), Cu1-S1 2.1882(18), S1-S2 2.070(2), N1-Cu1-N2 98.6(2), N1-Cu1-S1 131.15(15), N2-Cu1-S1 129.80(15).

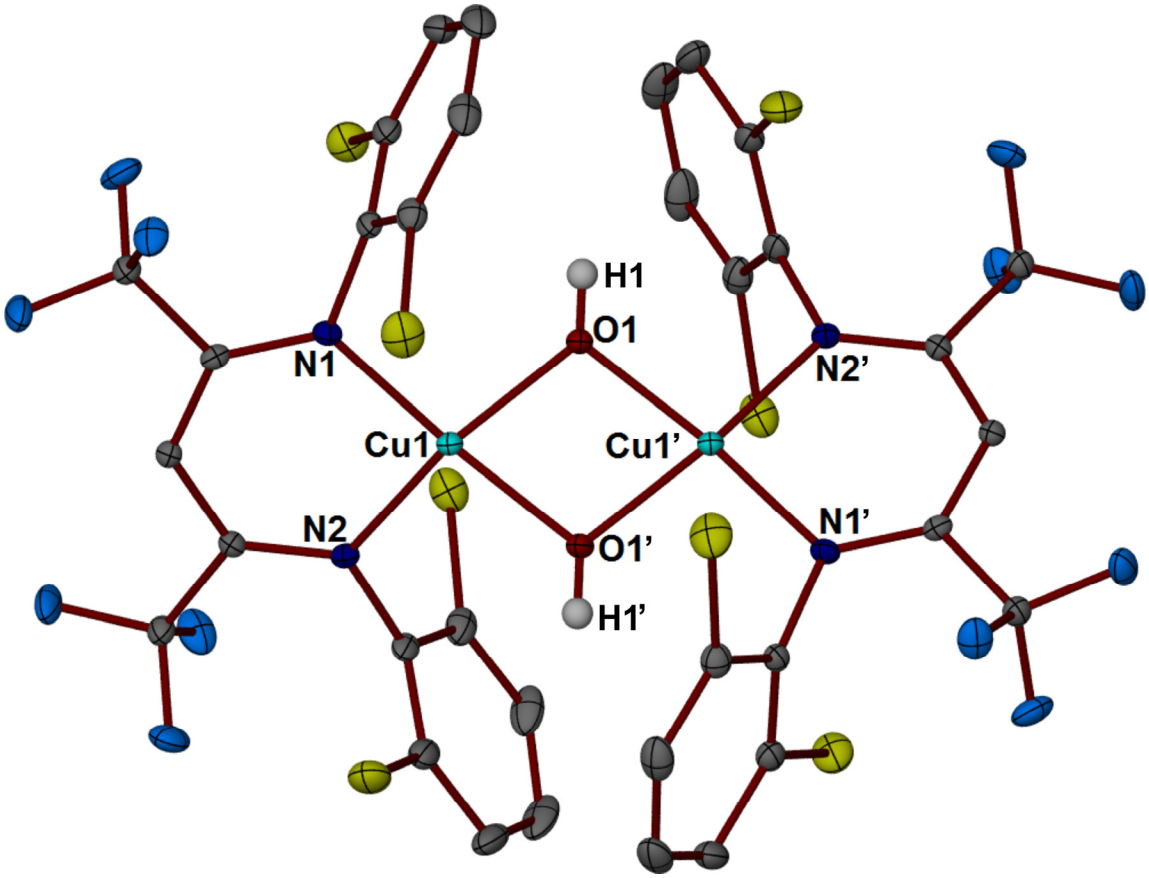

Figure S29. Molecular structure of $\{[Cl_2NN_{F6}]Cu\}_2(\mu\text{-}OH)_2$ (**4**) (CCDC 1513104). The thermal ellipsoid plots are drawn at 50% probability level. Cu1', N1', N2', O1', and H1' are symmetry generated atoms. Hydrogen atoms (except the hydroxo hydrogen atoms) are omitted for clarity. Selected bond distances (Å) and angles (°): Cu1-N1 1.9452(18), Cu1-N2 1.9466(18), Cu1-O1 1.9114(16), Cu1-O1' 1.9173(16), Cu1•••Cu1' 3.0145(5), N1-Cu1-N2 94.33(7), N1-Cu1-O1 98.41(7), N2-Cu1-O1' 97.15(7), O1-Cu1-O1' 76.02(7).

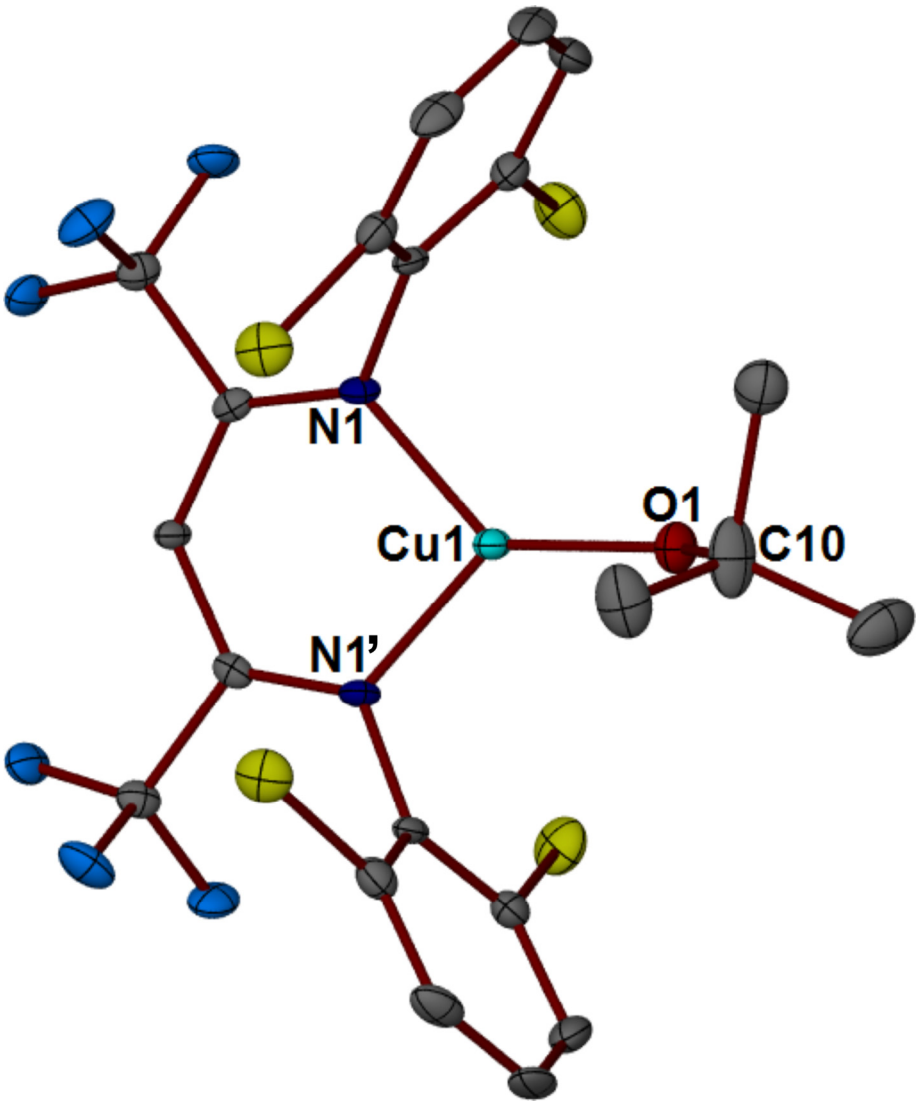

Figure S30. Molecular structure of $[Cl_2NN_{F6}]$Cu-O^{t}Bu (**6**) (CCDC 1513105). The thermal ellipsoid plots are drawn at 50% probability level. N1' is a symmetry generated atom. Hydrogen atoms are omitted for clarity. Only the major component of disordered sites is shown. Selected bond distances (Å) and angles (°): Cu1-N1 1.900(2), Cu1-N1' 1.900(2), Cu1-O1 1.756(3), O1-C10 1.404(5), N1-Cu1-N1' 95.81(12), N1-Cu1-O1 132.07(6), Cu1-O1-C10 127.1(2).

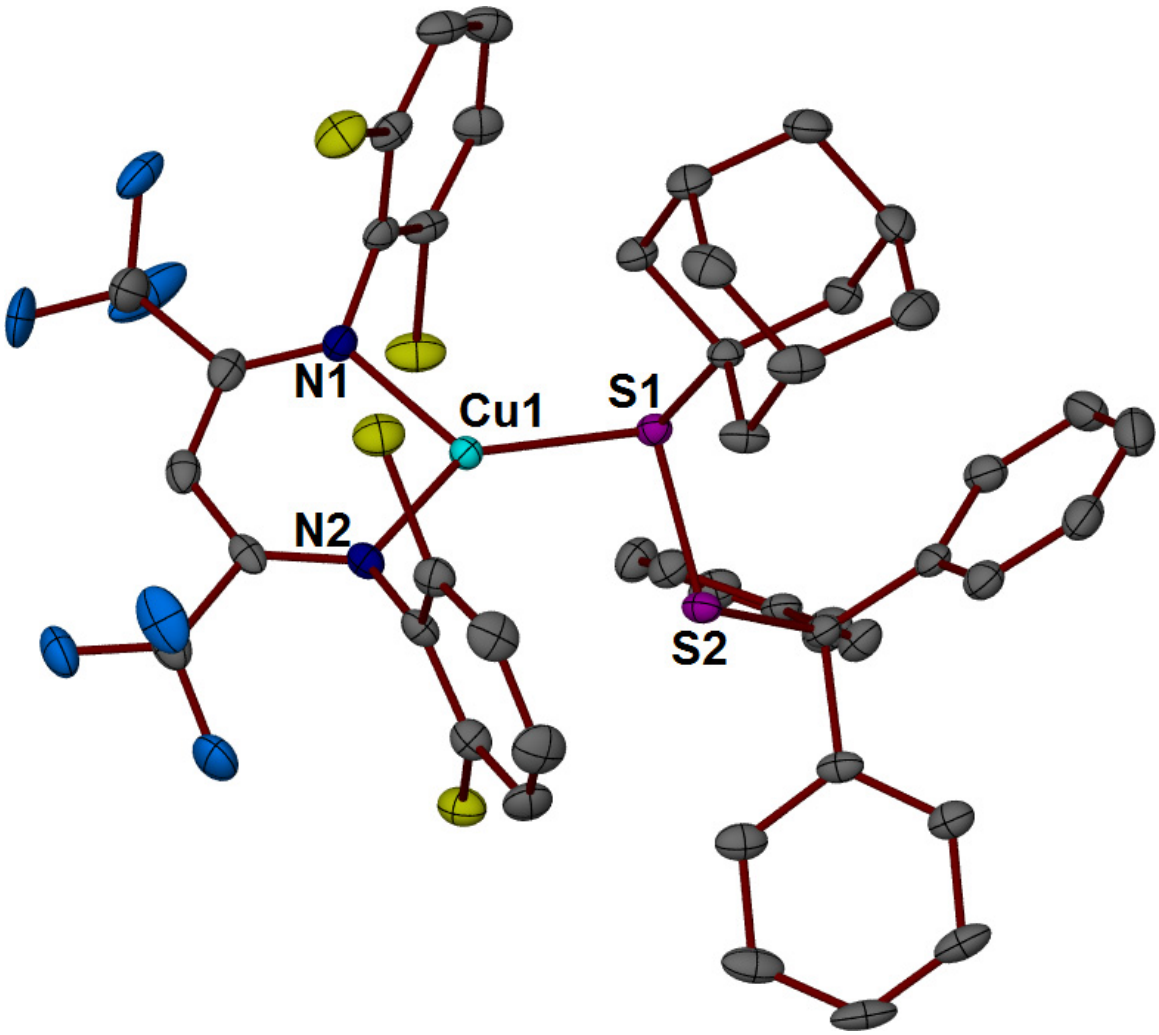

Figure S31. Molecular structure of $[Cl_2NN_{F6}]Cu(AdS\text{-}SCPh_3)$ ($\mathbf{3}^{\mathbf{AdCPh3}}$) (CCDC 1513103). The thermal ellipsoid plots are drawn at 50% probability level. Hydrogen atoms are omitted for clarity. Only the major component of disordered sites is shown. Selected bond distances (Å) and angles (°): Cu1-N1 1.976(2), Cu1-N2 1.941(2), Cu1-S1 2.2088(8), S1-S2 2.0601(9), N1-Cu1-N2 98.03(10), N1-Cu1-S1 121.53(7), N2-Cu1-S1 140.39(7).

19. References

(1) (a) Carey, D. T.; Cope-Eatough, E. K.; Vilaplana-Mafe, E.; Mair, F. S.; Pritchard, R. G.;Warren, J. E.; Woods, R. J. *Dalton Trans.* **2003**, 1083. (b) Bellows, S. M.; Brennessel, W. W.; Holland, P. L. *Eur. J. Inorg. Chem.* **2016**, 3344.

(2) Salvador, T. K.; Arnett, C. H.; Kundu, S.; Sapiezynski, N. G.; Bertke, J. A., Boroujeni, M. R.; Warren, T. H. *J. Am. Chem. Soc.* **2017**, DOI: 10.1021/jacs.6b09057.

(3) (a) Weston, R. E. Jr.; Brodasky, T. F. *J. Chem. Phys.* **1957**, *27*, 683. (b) Miller, F. A.; Wilkins, C. H. *Anal. Chem.* **1952**, *24*, 1253.

(4) Sanders, B. C.; Hassan, S. M.; Harrop, T. C. *J. Am. Chem. Soc.* **2014**, *136*, 10230.

(5) Pignolet, L. H., Lewis, R. A. Holm, R. H. *J. Am. Chem. Soc.* **1971**, *93*, 360.

(6) Cardenas, A. J. P.; Abelman, R.; Warren, T. H. *Chem. Commun.* **2014**, *50*, 168.

(7) Sarte, B., Stanford, J. Laprice, W. J., Uhrich, D. L., Lockhart, T. E., Gelerinter, E., Duffy, N. V. *Inorg. Chem.* **1978.** 3361**.**

(8) Williams, D. L. H. *Acc. Chem. Res.* **1999**, *32*, 869.

(9) Melzer, M. M.; Mossin, S.; Cardenas, A. J. P.; Williams, K. D.; Zhang, S.; Meyer, K.; Warren, T. H. *Inorg. Chem.* **2012**, *51*, 8658.

(10) Melzer, M. M.; Mossin, S.; Dai, X.; Bartell, A. M.; Kapoor, P.; Meyer, K.; Warren, T. H. *Angew. Chem. Int. Ed.* **2010**, *49*, 904.

(11) Holland, P. L.; Tolman, W. B. *J. Am. Chem. Soc.* **1999**, *121*, 7270.

(12) Gephart, R. T.; Mcmullin, C. L.; Sapiezynski, N. G.; Jang, E. S.; Aguila, M. J. B.; Cundari, T. R.; Warren, T. H. *J. Am. Chem. Soc.* **2012**, *134*, 17350.

(13) (a) SHELXTL-PC, Vers. 5.10; 1998, Bruker-Analytical X-ray Services, Madison, WI; (b) G. M. Sheldrick, SHELX-97, Universität Göttingen, Göttingen, Germany.

(14) L. Barbour, XSEED, 1999.

(15) SADABS; G. M. Sheldrick, 1996, based on the method described in R. H. Blessing, *Acta Crystallogr. Sect. A*, **1995**, *51*, 33.